


Summer 7-2019

Investigation of GRACE-derived Information on Forest Drought Stress Across the Contiguous US

Beichen Zhang

University of Nebraska - Lincoln, beichen@huskers.unl.edu

Follow this and additional works at: <https://digitalcommons.unl.edu/natresdiss>

 Part of the [Climate Commons](#), [Environmental Indicators and Impact Assessment Commons](#), [Environmental Monitoring Commons](#), [Hydrology Commons](#), [Meteorology Commons](#), [Natural Resources and Conservation Commons](#), and the [Other Environmental Sciences Commons](#)

Zhang, Beichen, "Investigation of GRACE-derived Information on Forest Drought Stress Across the Contiguous US" (2019).
Dissertations & Theses in Natural Resources. 294.
<https://digitalcommons.unl.edu/natresdiss/294>

This Article is brought to you for free and open access by the Natural Resources, School of at DigitalCommons@University of Nebraska - Lincoln. It has been accepted for inclusion in Dissertations & Theses in Natural Resources by an authorized administrator of DigitalCommons@University of Nebraska - Lincoln.

INVESTIGATION OF GRACE-DERIVED INFORMATION ON FOREST DROUGHT
STRESS ACROSS THE CONTIGUOUS US

by

Beichen Zhang

A THESIS

Presented to the Faculty of
The Graduate College at the University of Nebraska
In Partial Fulfilment of Requirements
For the Degree of Master of Science

Major: Natural Resource Sciences

Under the Supervision of Professor Tsegaye Tadesse

Lincoln, Nebraska

July, 2019

INVESTIGATION OF GRACE-DERIVED INFORMATION ON FOREST DROUGHT
STRESS ACROSS THE CONTIGUOUS US

Beichen Zhang, M.S.

University of Nebraska, 2019

Adviser: Tsegaye Tadesse

This research derives z-score monthly groundwater storage (GWS) anomalies and z-score monthly root zone soil moisture (RZSM) anomalies from products of Gravity Recovery and Climate Experiment Data Assimilation (GRACE-DA). Z-score monthly GWS and RZSM anomalies are compared to two drought indicators: Standardized Precipitation Index (SPI) and Standardized Precipitation-Evapotranspiration Index (SPEI) to investigate the usefulness of GRACE-DA information to detect drought conditions at tree-ring sites. This study also compares z-score monthly GWS and RZSM anomalies with the Tree Ring Standardized Growth Index (TRSGI) that is resampled by bootstrapping to investigate the capability of monitoring forest drought stress. Finally, this research uses multiple linear regression to develop a model for predicting tree-ring widths at selected study sites.

The results of the comparisons of z-score monthly GWS and RZSM anomalies and commonly-used drought indices (SPI and SPEI) indicate that GWS anomalies have strong correlations (> 0.4) with long-term droughts (> 9 months) and RZSM anomalies have strong correlations (> 0.5) with short-term droughts (< 3 months). The results of comparisons of TRSGI suggest that z-score monthly GWS and RZSM anomalies are significantly related to tree-ring widths with a significant level of 0.05. This research suggests that the relationships between GWS anomalies and drought indices (SPI and SPEI) and TRSGI highly depend on the geological formations, such as the types of the aquifers, and geographical environments such as the soil texture. The multiple linear regression in this paper quantifies the impacts of

z-score monthly GWS and RZSM anomalies on tree-ring widths, which suggests GRACE-DA products can provide useful information to detect and predict the growth of trees. The results also suggest the predictor, monthly RZSM anomalies, is one of the most important parameters in the regression model. Overall, the study suggests that GRACE-DA information can be used to help detect and monitor the stress from drought impacts on trees at a large spatial scale.

ACKNOWLEDGMENTS

This research becomes a reality with the kind support and help of many faculties and professors in the School of Natural Resources and the Department of Statistics. I would like to express my sincere thanks to all of them. Foremost, I would like to thank my committee members: Dr. Brian Wardlow, Dr. Michael Hayes, Dr. Tsegaye Tadesse, and Dr. Yuzhen Zhou, for sharing their valuable time and experience with me. They not only professionally and patiently answered my questions during the research but also provided useful suggestions for my academic development. I want to give a special thank to my advisor Dr. Tsegaye Tadesse. His guidance and encouraged me in all the time of research and helped me have a deeper understanding of rigorous research. I would like to express my gratitude to Dr. Eric North, Dr. Getachew Demisse, Dr. Yared Bayissa, Curtis Riganti, and other people who gave me comments and helps in the research. I would also like to thank the National Drought Mitigation Center (NDMC) for the financial support of my study.

Furthermore, I would like to thank the High Plains Regional Climate Center (HPRCC), NDMC, International Tree-Ring Data Bank (ITRDB), and National Aeronautics and Space Administration (NASA)/ Goddard Space Flight Center (GSFC) for making datasets public. I would specially thank Hiroko Beaudoin for providing generous helps with GRACE-DA products.

At last, I would like to acknowledge with gratitude to my family, and friends for mental and spiritual supports in this period. Thank you to my parents and girlfriend. Your love and supports would always keep me going.

GRANT INFORMATION

This research was partially supported by three NOAA projects which allowed me to attend graduate school:

Drought information services for agriculture across the United States 2018-2019

Award No. 58-0111-18-018

Drought information services and research for agriculture across the United States

Award No. 58-0111-17-013

Providing drought information services for the nation: the National Drought Mitigation Center

Award No. NA15OAR4310110

Table of Contents

List of Figures	viii
List of Tables	xii
1 INTRODUCTION	1
1.1 Motivation	1
1.2 Background	3
1.2.1 Drought	3
1.2.2 GRACE	6
1.2.3 Tree Rings	9
2 DATA AND METHODOLOGY	11
2.1 Data Descriptions and Processing	11
2.1.1 Monthly Anomalies Derived from GRACE-DA Products	11
2.1.2 Standardized Precipitation Index (SPI)	14
2.1.3 Standardized Precipitation Evapotranspiration Index (SPEI)	16
2.1.4 Tree Ring Standardized Growth Index (TRSGI)	16
2.1.5 Normalized Difference Vegetation Index (NDVI)	20
2.2 Statistical Methods	22
2.2.1 Simple Linear Correlation	22
2.2.2 Bootstrapping	23

2.2.3	Multiple Linear Regression	23
3	Results and Discussion	26
3.1	Correlation between monthly GWS anomalies and drought indices (SPI and SPEI)	26
3.2	Correlation between monthly RZSM anomalies and drought indices (SPI, SPEI)	33
3.3	Comparison between monthly GWS anomalies and TRSGI	37
3.4	Comparison between monthly RZSM anomalies and TRSGI	42
3.5	Multiple linear regression analysis	45
3.5.1	Variable Selection	46
3.5.2	Model Diagnostics	48
3.5.3	Model Validation	50
4	Conclusions	54
A	Time Series Plots of monthly GWS anomalies, SPI, and SPEI at az597, az587 and or092	58
B	Comparison between drought indices (SPI and SPEI) and TRSGI	63
	References	64

List of Figures

2.1	Example of z-score monthly GWS anomalies in July 2012	13
2.2	Example of z-score monthly RZSM anomalies in July 2012	14
2.3	Distribution of tree-ring sites across the CONUS and the nine forest divisions: Northwest, West, West North Central, Southwest, South, East North Central, Central, Southeast, and Northeast	17
3.1	Boxplot of correlation coefficients between GWS anomalies and SPI in 3-month, 6-month, 9-month, 12-month, 18-month, 24-month accumulation periods for the 34 tree-ring sites, where the black circles show the outliers	28
3.2	Boxplot of correlation coefficients between GWS anomalies and SPEI in 3-month, 6-month, 9-month, 12-month, 18-month, 24-month accumulation periods for the 34 tree-ring sites, where the black circles show the outliers	30
3.3	Maps showing the spatial patterns of correlations between GWS anomalies and SPI at 34 sites. The radius of the symbol represents the correlation coefficient. A larger circle stands for a higher correlation. (a) GWS-SPI3, (b) GWS-SPI6, (c) GWS-SPI9, (d) GWS-SPI12, (e) GWS-SPI18, (f) GWS-SPI24	31
3.4	Maps showing the spatial patterns of correlations between GWS anomalies and SPEI at 34 sites. The radius of the symbol represents the correlation coefficient. A larger circle stands for a higher correlation. (a) GWS-SPEI3, (b) GWS-SPEI6, (c) GWS-SPEI9, (d) GWS-SPEI12, (e) GWS-SPEI18, (f) GWS-SPEI24	32

3.5	Boxplot of correlation coefficients between RZSM anomalies and SPI in 3-month, 6-month, 9-month, 12-month, 18-month, 24-month accumulation periods for the 34 tree-ring sites, where the black circles show the outliers	35
3.6	Maps showing the spatial patterns of correlations between RZSM anomalies and SPI at 34 sites. The radius of the symbol represents the correlation coefficient. A larger circle stands for a higher correlation. (a) RZSM-SPI3, (b) RZSM-SPI6, (c) RZSM-SPI9, (d) RZSM-SPI12, (e) RZSM-SPI18, (f) RZSM-SPI24	36
3.7	Boxplot of correlation coefficients between RZSM anomalies and SPEI in 3-month, 6-month, 9-month, 12-month, 18-month, 24-month accumulation periods for the 34 tree-ring sites, where the black circles show the outliers	38
3.8	Maps showing the spatial patterns of correlations between RZSM anomalies and SPEI at 34 sites. The radius of the symbol represents the correlation coefficient. A larger circle stands for a higher correlation. (a) RZSM-SPEI3, (b) RZSM-SPEI6, (c) RZSM-SPEI9, (d) RZSM-SPEI12, (e) RZSM-SPEI18, (f) RZSM-SPEI24	39
3.9	The heatmap showing the correlations between month GWS anomalies and resampled TRSGI in ten states, where grey represents insignificant correlations, and brown represents high correlations and black represents low correlations.	40
3.10	The heatmap showing the correlations between month RZSM anomalies and resampled TRSGI in ten states, where grey represents insignificant correlations, brown and black represents high positive and negative correlations respectively, and brighter color represents lower correlation	43
3.11	The scatterplot showing relationships between every two variables	47

3.12	Diagnostic plots for the proposed model. (a) standardized residual plot of SPEI9 (b) standardized residual plot of RZSM anomalies (c) standardized residual plot of fitted value (fitted TRSGI) (d) Scatterplot where the x-axis is fitted TRSGI and the y-axis is actual TRSGI (e) square root plot where the x-axis is fitted TRSGI (f) normal Q-Q plot	51
3.13	The Profile of Log-likelihood for Box-Cox Transformations	52
3.14	Diagnostic plots for the new model. (a) standardized residual plot of SPEI9 (b) standardized residual plot of RZSM anomalies (c) standardized residual plot of fitted value (fitted TRSGI) (d) Scatterplot where the x-axis is fitted TRSGI and the y-axis is actual TRSGI (e) square root plot where the x-axis is fitted TRSGI (f) normal Q-Q plot	53
A.1	The time series plot of monthly GWS anomalies and SPI3 at sites az597 and az598 (they are at a same location)	58
A.2	The time series plot of monthly GWS anomalies and SPI6 at sites az597 and az598 (they are at a same location)	59
A.3	The time series plot of monthly GWS anomalies and SPI9 at sites az597 and az598 (they are at a same location)	59
A.4	The time series plot of monthly GWS anomalies and SPI12 at sites az597 and az598 (they are at a same location)	59
A.5	The time series plot of monthly GWS anomalies and SPI18 at sites az597 and az598 (they are at a same location)	60
A.6	The time series plot of monthly GWS anomalies and SPI24 at sites az597 and az598 (they are at a same location)	60
A.7	The time series plot of monthly GWS anomalies and SPI3 at the site or094 . . .	60
A.8	The time series plot of monthly GWS anomalies and SPI6 at the site or094 . . .	61

A.9	The time series plot of monthly GWS anomalies and SPI9 at the site or094 . . .	61
A.10	The time series plot of monthly GWS anomalies and SPI12 at the site or094 . .	61
A.11	The time series plot of monthly GWS anomalies and SPI18 at the site or094 . .	62
A.12	The time series plot of monthly GWS anomalies and SPI24 at the site or094 . .	62
B.1	The heatmap showing the correlations between drought indices (SPI and SPEI) and resampled TRSGI in ten states, where grey represents insignificant correlations, brown and black represents high positive and negative correlations respectively, and brighter color represents lower correlation	63

List of Tables

2.1	The distance between tree sites and weather stations, descending by the distance	15
2.2	The table describes the locations of tree sites and species and ages of trees . . .	18
2.3	The table describes geographic environments of tree sites which include longitude and latitude, elevation, slope, available water content (AWC), and soil texture . .	19
2.4	The monthly mean NDVI ratio for each national forest region	21
3.1	The mean, median, minimum, and maximum of correlation coefficients between GWS anomalies and SPI in 3-month, 6-month, 9-month, 12-month, 18-month, 24-month accumulation periods for the 34 tree-ring sites	27
3.2	The mean, median, minimum, and maximum of correlation coefficients between GWS anomalies and SPEI in 3-month, 6-month, 9-month, 12-month, 18-month, 24-month accumulation periods for the 34 tree-ring sites	29
3.3	The mean, median, minimum, and maximum of correlation coefficients between RZSM anomalies and SPI in 3-month, 6-month, 9-month, 12-month, 18-month, 24-month accumulation periods for the 34 tree-ring sites	34
3.4	The mean, median, minimum, and maximum of correlation coefficients between RSZM anomalies and SPEI in 3-month, 6-month, 9-month, 12-month, 18-month, 24-month accumulation periods for the 34 tree-ring sites	37

3.5	The mean, median, minimum, and maximum of correlation coefficients between RSZM anomalies and SPEI in 3-month, 6-month, 9-month, 12-month, 18-month, 24-month accumulation periods	46
3.6	The mean, median, minimum, and maximum of correlation coefficients between RSZM anomalies and SPEI in 3-month, 6-month, 9-month, 12-month, 18-month, 24-month accumulation periods	48
3.7	The mean, median, minimum, and maximum of correlation coefficients between RSZM anomalies and SPEI in 3-month, 6-month, 9-month, 12-month, 18-month, 24-month accumulation periods	48

Chapter 1

INTRODUCTION

1.1 Motivation

In recent years, the frequency and severity of drought extremes associated with global climate change are increasing. Economic, social, and environmental damages and costs from droughts are growing significantly as well (Wilhite, 2000; Wilhite et al., 2014). Droughts arise in almost all forest ecosystems. With atmospheric moisture demand rising under a drought condition, higher evapotranspiration and lower soil moisture would increase water stress on trees (Dale et al., 2001; Allen et al., 2015; Bhuyan et al., 2017). In some regions where the water table is near the soil column, groundwater recharging and discharging could have notable impacts on soil moisture (Chen and Hu, 2004). Quantifying the relationship between soil moisture and groundwater in forest areas is critical for monitoring long-term forest drought stress, forest management, and drought recovery.

The growth of trees is sensitive to diverse local climates and the yearly time series of effects from the changing environment (temperature, precipitation) are conscientiously recorded by the sequence of tree rings in trees. Comparing modern climate records with the tree-ring widths during in the same period and establishing a mathematical equation for the relationship between them can calibrate modeled climate data and provide valuable information such as the importance of different climate variables for the forestry

management(Fritts, 2012).

The Gravity Recovery and Climate Experiment Data Assimilation (GRACE-DA) products are processed by the National Aeronautics and Space Administration (NASA) Goddard Space Flight Center (GSFC). The GRACE observations are used as inputs to a data assimilation framework built upon the Catchment Fortuna 2.5 land surface model, which produces a result of 35 variables per day. Terrestrial water storage, soil moisture content, and snow water equivalent are three main products. These products are the most recent satellite-derived datasets that can help in monitoring variations of forest-level soil moisture and groundwater over time.

The primary objective of this study is to assess the monthly anomalies of the subsurface water storage that are derived from GRACE-DA as integrated drought impacts and comparing them with the Standardized Precipitation Index (SPI), the Standardized Precipitation-Evapotranspiration Index (SPEI) and the Tree-ring Standardized Growth Index (TRSGI) across the Contiguous United States (CONUS) from 2003 to 2010. Specifically, the objectives of this study to investigate the value of GRACE-DA products for drought monitoring over forests include: (1) examining the patterns between TRSGI and GRACE-DA products to understand the spatial and temporal patterns of forests response to drought at multiple time scales (from 3 months to 24 months) and (2) understanding relationships among GRACE-DA products and commonly-used drought indicators (SPI and SPEI), which represents to analyze major components of the water cycle related to drought that include precipitation, evapotranspiration, soil moisture, and groundwater, hence contributing to monitor forest drought stress.

1.2 Background

1.2.1 Drought

Drought is considered as one of the most complex natural hazards and causes broad impacts. The development of drought is usually slow, and the impacts accumulate over a substantial period. It is difficult to determine the onset and end of a drought. Although drought is a common phenomenon for all climate regimes, there is not an exact definition of drought. Definitions of drought depend highly on regional environments and the sector of impacts, determining the extent of droughts that can spread over larger spatial areas and the impacts that are less evident than other natural disasters. Therefore, tasks to quantitatively monitor and predict the formation and impacts of drought are crucial but challenging (Wilhite, 1993).

Drought is generally defined as the consequence of persistent deficits of precipitation over a prolonged period in a specific region (Wilhite, 1993; Zargar et al., 2011). However, the types of drought vary by temporal and spatial extent, intensity, and the demands made by vegetation and human activities. Wilhite and Glantz (1985) grouped droughts into four types as follow: meteorological, hydrological, agricultural, and socioeconomic. Meteorological drought is solely determined by the level of dryness (deficits between the average and normal amount of precipitation) and the duration of the period in a specific region. Agricultural drought is a result of various effects of meteorological drought which includes but not limited to low soil moisture, high temperature, and high vapor pressure deficits. Hydrological drought develops out of the shortage of surface or subsurface water supply (i.e., groundwater, soil moisture, streamflow, reservoir, and lake levels). It usually lags the occurrence of both meteorological and agricultural drought. Socioeconomic drought links the supply and demand for economic goods and services that are related to meteorological, hydrological, and agricultural droughts. It occurs when the demand exceeds the supply, which is a result of

weather-related deficits in the water supply (Wilhite and Glantz, 1985). By these definitions, water is the most critical factor in all kinds of drought, and monitoring changes of water is a primary objective to all relevant studies.

Drought has multiple impacts on forests. Physiological and morphological characteristics of trees have changed to adapt in regions where seasonal droughts are common. In areas where drought is less common, responses of forests can be substantial since the forest ecosystems are not well adapted to drought conditions. Vulnerability to drought differs by species as consequences of differences in their biophysical attributes of the root, xylem, and mycorrhizal. In general, the effects of high vapour-pressure deficits and soil moisture deficits combined with high temperature provoke stress of forest, leading to carbon stress, the disorder of hydraulic function, and even mortality (Vose et al., 2016).

The ecological functions and services of forests are progressively rising in the United States and around the world. Forests can protect the watershed and prevent soil erosion. After oceans, forests are the second vast storehouses of carbon in the world that can offset 10%-40% of annual carbon emissions each year (Sun et al., 2015). Due to climate change, the severity and intensity of drought are anticipated to increase in the future (IPCC, 2018). Dynamic changes of drought and complex mechanisms of responses in forest ecosystems make it challenging to analyze the relationships between forest water supply and productivity at large scales (Sun et al., 2015). Hence, understanding how drought affects forests becomes essential and necessary.

Various techniques have been used to quantify the responses of forests to water stress and drought. Analyzing relationships between drought indices at multiple time scales and different variables that can reflect the growing status of trees becomes a prevalent and robust approach (Williams et al., 2012; Babst et al., 2013; Vicente-Serrano et al., 2014; Ogaya et al., 2015; Sun et al., 2015; Bhuyan et al., 2017; Gao et al., 2018). In these prior studies, temperature, precipitation, and potential evapotranspiration are considered

as the three most widely used variables to compare with the growth of trees. Some studies have also used drought indices such as the Palmer Drought Severity Index (PDSI) (Bhuyan et al., 2017), self-calibrating Palmer Drought Severity Index (scPDSI) (Bhuyan et al., 2017), Standardized Precipitation Index (SPI) (Bhuyan et al., 2017), and Standardized Precipitation-Evapotranspiration Index (SPEI) (Vicente-Serrano et al., 2014; Bhuyan et al., 2017).

The PDSI (Palmer, 1965) was developed to measure the severity of meteorological drought and wet situations. It is widely used in the U.S. and works effectively on monitoring seasonal to long-term droughts. Eight variables related to soil moisture are computed based on temperature, precipitation, and available water holding capacity of the soil that include evapotranspiration, recharge, runoff, potential evapotranspiration, potential recharge, potential runoff, and potential loss (Wells et al., 2004; Zargar et al., 2011).

The scPDSI is similar to the PDSI except for replacing all empirical constant coefficients in Palmer's equation with values calculated based upon the site-specific climatic data. Compared with the PDSI, the scPDSI improves the statistical accuracy under severe and extreme droughts and allows the comparison between different locations and times (Wells et al., 2004).

The calculation of SPI is only based on precipitation. Precipitation records within a moving window are compared with the same period in the historical records. The moving window can be any period of length. 3, 6, 9, 12, 24, and 48-month periods are the most common. Values are first fitted to a Gamma distribution that is then transformed into a normal distribution by calculating the cumulative probability. Because aggravated precipitation deficits in different periods are influenced by various water resources (e.g., snowpack, soil moisture, groundwater), the various durations can be utilized to reflect the change in different water features. For example, a 1-month SPI can efficiently monitor short-term changes of soil moisture and crop stress in the growing season while a 12-month SPI performs higher

correlations with stream flows, reservoir levels, and groundwater. The SPEI is calculated from deficits of precipitation and potential evapotranspiration for multiple timescales. The process of the SPEI calculation is similar to SPI, except that the deficits are fitted to the log-logistic distribution (Bayissa et al., 2015; Bayissa et al., 2017).

Previous studies indicate that the behavior of the scPDSI is similar to the long-term SPI and SPEI (9 months to 12 months). In addition, scPDSI, SPI, and SPEI all have significant correlations with tree-ring width index data at long time scales (Vicente-Serrano et al., 2014; Bhuyan et al., 2017). Although these studies have directly or indirectly considered the effects of soil moisture, the impacts of groundwater and deep soil moisture are omitted. Groundwater has significant implications on soil moisture of the root zone in the areas where the groundwater table is near the surface (Chen and Hu, 2004). Since large woody tree roots are primarily located within 1 to 2 meters (Perry, 1989), correctly considering relationships between tree growth and deep soil moisture and groundwater is crucial to improving our understanding how the water stress of trees is related to and affected by the groundwater variations.

1.2.2 GRACE

Launched in March 2002, the GRACE mission is designed to measure variations of Earth's gravity field. It includes two satellites that fly in an Earth Polar Orbit at an approximate distance of 220 km (137 miles). Using the global positioning system (GPS) and a microwave ranging system, GRACE can detect changes of Earth's gravitational by accurately measuring the distance between the two orbiters. Beyond static spatial variations that are caused by geological features such as large mountain ranges, the gravity variations over time are mainly attributed to four parts: ocean, runoff and groundwater, ice, and mass within Earth. This mission also aims to improve the profile of Earth's atmosphere (NASA, 2003; Tapley et al., 2014). Due to battery failure of one satellite, the GRACE mission

concluded in October 2017. GRACE revolutionize investigations and quantification of mass trends and fluctuations, providing over 163 months of data of variations in the Earth's gravity field. In May 2018, the GRACE Follow-On (GRACE-FO) mission was successfully launched. GRACE-FO will continue data collection with a potential to increase the spatial and temporal resolution and the accuracy of the satellite-to-satellite distance with evolved versions of GRACE instrumentation (Tapley et al., 2019).

GRACE data are processed at three institutions including the University of Texas Center for Space Research (CSR), the GeoForschungsZentrum Potsdam (GFZ), and the NASA Jet Propulsion Laboratory (JPL), respectively. Although processing algorithms are different in each center, the critical characteristics of procedures are the same. The effects of the atmosphere and oceans are removed by several designed filters. The remaining signals from the monthly GRACE observations are mostly related to variations of terrestrial water storage (TWS) (Landerer and Swenson, 2012). The TWS is the sum of surface water, soil moisture, groundwater, ice and snow, and biomass and has addressed the gap of monitoring water storage variations at a large scale on a systematic basis. TWS has been used for studying freshwater discharge, evapotranspiration, the mass balance of ice, water balance of lakes, and extreme hydrological drought events (Houborg et al., 2012). While GRACE has provided valuable data for climatic and hydrological studies, monthly temporal resolution and coarse horizontal spatial resolution of 150,000 km² are obstacles to advanced studies and applications that require higher resolutions (Rowlands et al., 2005; Yeh et al., 2006). Besides, TWS shows the changes in integrated water from groundwater to biomass and ice and snow, representing an entire vertical column of water. Assimilating GRACE TWS with the simulated land surface model (LSM) is utilized to disaggregate GRACE observations in many studies. A few prior studies (Zaitchik et al., 2008; Su et al. 2010; Houborg et al., 2012; Eicker et al., 2014; Tangdamrongsub et al., 2015; Kumar et al., 2016; Khaki et al., 2017) have explored the use of GRACE TWS data for data assimilation.

Among the LSMs, the Catchment Land Surface Model (CLSM; Koster et al., 2000; Ducharne et al., 2000) is the only one in the North American and Data Assimilation System (NLDAS; Mitchell et al., 2004) that can simulate variations of unconfined groundwater storage, which typically 2-3 meter below the land surface (Houborg et al., 2012; Kumar et al., 2016). CLSM defines the fundamental surface as hydrological catchments, instead of the land surface, at the grid scale. There are three subsurface variables within each catchment: catchment deficit, root zone excess, and surface excess, which simulates changes of water at different vertical depths (Koster et al., 2000). These characteristics of CLSM make it especially appropriate for the data assimilation with GRACE TWS. Therefore, Zaichik and his research team assimilate monthly GRACE-derived TWS observations with CLSM by using the ensemble Kalman filter and smoothers.

Several studies show that the assimilation of GRACE TWS with CLSM can contribute to drought applications and GRACE-based drought indicators are developed to improve drought detection and monitoring (Houborg et al., 2012; Li et al., 2012; Thomas et al., 2017). First, GRACE TWS data have been downscaled in spatial and temporal resolutions and disaggregated vertically into U.S. Drought Monitor products, address gaps of investigating groundwater and soil moisture at a larger scale. GRACE TWS data assimilation products can provide useful independent information that can improve the accuracy of soil moisture estimations in the Eastern U.S. (Houborg et al., 2012). Additionally, a Groundwater Drought Index (GWI) derived from GRACE TWS data assimilation products demonstrates that GRACE improves correlations with GWI based in situ data as compared with other model-based groundwater drought indices, indicating that GRACE data assimilation products can improve groundwater storage estimations at a regional scale (Li and Rodell, 2014). Therefore, this research utilizes GRACE-derived TWS data assimilation outputs to calculate anomalies of GWS and RZSM, which are compared with forest drought stress and other drought indices (SPI and SPEI).

1.2.3 Tree Rings

Tree rings are universally known as one of the most robust proxies for tree vitality (Dobbertin, 2005; Fritts et al., 2012; Ma et al., 2015; Bhuyan et al., 2017), and directly connect with climate events such as drought. Temperature and water are two primary climatic variables that restrict the growing period of trees, which hence affects the biomass of trees and the tree-ring width. The temperature has a significant influence on tree-ring growth at the beginning of the growing season. If the temperature decreases to an abnormal level as compared with the historical record, it will lead to a delay in the start of the growing season. Once the temperature increases and summer begins, water becomes the most critical climatic variable that accounts for a large amount of tree-ring width variations. High temperature and evaporative demands, combined with low soil moisture, can limit the cell division and cell enlargement processes (Fritts et al., 2012).

dendroclimatology is the science of studying past climates using tree-ring data. The effects of water stress depend upon not only the severity and duration of droughts but also the ages and species of trees. In dendroclimatology, standardization of tree-ring width is a necessary procedure to correct the effects of changing age and geometry of the tree from the measurements of tree-ring width in dendroclimatology. After the data are standardized, the values are called ring-width indices. The indices are unitless with a mean value of one. Generally, they have no linear trend and there are more fluctuations when a tree is in the younger fast-growing period as compared with the older slow-growing period (Fritts et al., 2012).

This research aims to investigate the relationship between monthly anomalies of the subsurface water storage derived from GRACE-DA products and a tree ring standardized growth index (TRSGI), using the Pearson correlation and multiple linear regression models to investigate the impacts of the subsurface water storage, precipitation, evapotranspiration

and temperature on tree growth under drought and non-drought conditions. The results from previous studies of GRACE TWS data assimilation products such as root zone soil moisture and groundwater storage indicate a potential of GRACE-DA products on the hydrological drought monitoring (Houborg et al., 2012; Li and Rodell, 2014; Thomas et al., 2017). Additionally, a few studies are evaluating the correlation between drought indices and tree-ring indices that support the concept that long-term observation records of SPI and SPEI can reflect the water stress of trees (Vicente-Serrano et al., 2014; Bhuyan et al., 2017; Gao et al., 2018). However, these studies omit the consideration of effects of hydrological drought (e.g., decreasing of the groundwater level). Quantification of the relationship between GRACE-DA products and the tree-ring widths is useful to investigate the impacts of a larger scale drought on forests and how subsurface water storage affects the growth of trees. This study analyzes the relationships between GRACE-DA products and drought indices (SPI and SPEI), investigating the GRACE-DA products as predictors for the forest drought stress and indicating the importance of subsurface water storage in forest drought stress monitoring.

Chapter 2

DATA AND METHODOLOGY

2.1 Data Descriptions and Processing

2.1.1 Monthly Anomalies Derived from GRACE-DA Products

This study calculates monthly anomaly data sets from GRACE-DA products. GRACE-DA products are processed from 0.5-degree gridded GRACE solutions from the University of Texas by assimilating with the Catchment Fortuna-2.5 land surface model, which increases bedrock depths by 3 meters ("readme", 2017). After data assimilation, the temporal resolution of GRACE-DA products is daily, and the spatial resolution is 0.125 degree. This study converts the daily temporal resolution to monthly to reduce variations. Monthly anomalies of root zone soil moisture are derived from root zone soil moisture (RZSM) in the soil profiles (0-100 centimeter) of the GRACE-DA products. The GRACE-DA products used in this study are from April 2002 to December 2017. Equation (2.1) calculates mean values of root zone soil moisture for each month, where i represents months in a year, j represents years from 2002 to 2017. For i in the range from April to December, j starts from 2002. For i in January, February, and March, j starts from 2003.

$$\overline{RZSM}_i = \frac{1}{2017 - J + 1} \sum_{j=J}^{2017} RZSM_i \quad (2.1)$$

Monthly anomalies are calculated to explore how root zone soil moisture affects tree-ring width by Equation (2.2). Hence, z-score values are used to standardize monthly anomalies of root zone soil moisture from 2003 to 2017 (Equation (2.3) and (2.4)). The monthly RZSM anomalies in 2002 are not included in the z-score calculation since complete datasets in years are required to compare with the annual ring-width index.

$$RZSM_D = RZSM - \overline{RZSM}_i \quad (i \in (1, 12)) \quad (2.2)$$

$$\overline{RZSM}_{Di} = \frac{1}{15} \sum_{i=2003}^{2017} RZSM_{Di} \quad (i \in (1, 12)) \quad (2.3)$$

$$RZSM_{Z-score} = \frac{RZSM_D - \overline{RZSM}_{Di}}{\sigma_{RZSM_{Di}}} (i \in (1, 12)) \quad (2.4)$$

Since the depth of large woody tree roots can be over 1 meter, this study also calculates groundwater storage (GWS) based on prior studies (Scanlon et al., 2012; Long et al., 2013). GWS in this research represents all subsurface water storage below 1-meter depth. Equation (2.5) shows how GWS is calculated from terrestrial water storage (TWS), snow water equivalent (SWE), and RZSM.

$$\Delta GWS = \Delta TWS - \Delta RZSM - \Delta SWE \quad (2.5)$$

The monthly GWS anomalies and z-score monthly GWS anomalies are calculated in the same procedure as RZSM (Equation (2.6), (2.7), (2.8), and (2.9)).

$$\overline{GWS}_i = \frac{1}{2017 - J + 1} \sum_{j=J}^{2017} GWS_j \quad (2.6)$$

$$GWS_D = GWS - \overline{GWS}_i \quad (i \in (1, 12)) \quad (2.7)$$

$$\overline{GWS}_{Di} = \frac{1}{15} \sum_{i=2003}^{2017} GWS_{Di} \quad (i \in (1, 12)) \quad (2.8)$$

$$GWS_{Z-score} = \frac{GWS_D - \overline{GWS}_{Di}}{\sigma_{GWS_{Di}}} (i \in (1, 12)) \quad (2.9)$$

Z-score monthly RZSM anomalies and Z-score monthly GWS anomalies are produced at 0.125-degree spatial resolution, which is approximately equal to 11.3*11.3 km in the Conus Albers projection system from January 2003 to December 2017. Since observations of tree-ring data terminated in 2010, a study period of 2003 to 2010 are utilized to compare with the GRACE information with other drought indices. Figure 2.1 and Figure 2.2 are examples for the z-score monthly GWS anomalies and the z-score monthly RZSM anomalies in July 2012. All these procedures are done by python scripts with the package GDAL.

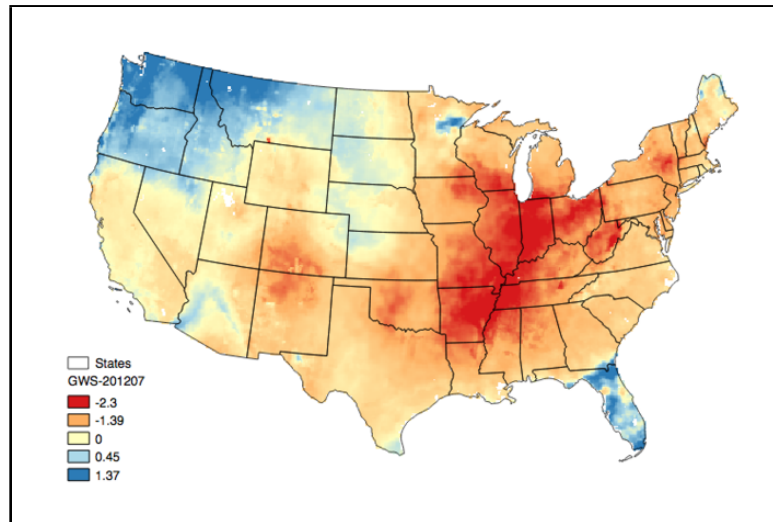


Figure 2.1: Example of z-score monthly GWS anomalies in July 2012

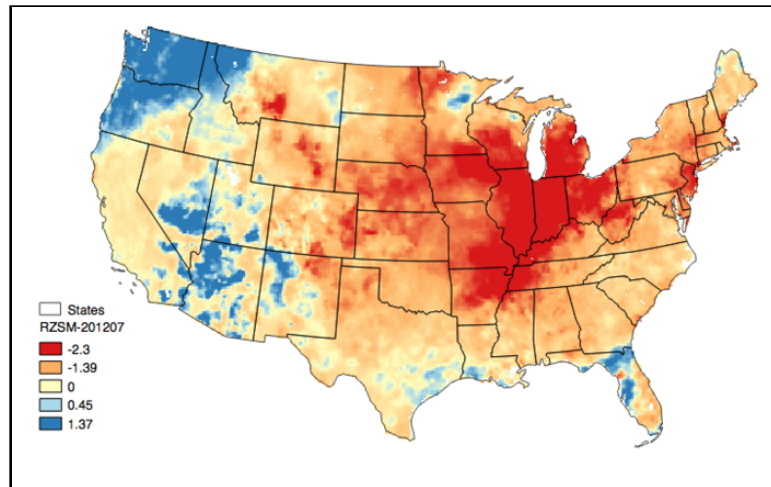


Figure 2.2: Example of z-score monthly RZSM anomalies in July 2012

2.1.2 Standardized Precipitation Index (SPI)

SPI represents the standardized precipitation deficits between a period of i months (in this study, $i = 3, 6, 9, 12, 18, 24$) and the same period in historical records (McKee et al., 1993). The daily historical precipitation records at twenty-five weather stations from 1970 to 2016 are collected from the High Plains Regional Climate Center (HPRCC). This study calculates the distance between the weather stations and the tree sites. The precipitation dataset from the nearest stations is used to calculate the index. The nearest distances are varied from 0.013 to 0.787 degree (approximately from 1.43 to 85.8 km) and are listed in Table 2.1. The study uses the SPI Generator application, which is released by the National Drought Mitigation Center (NDMC). The generator reads a precipitation record and outputs monthly SPI data in multiple accumulative periods. Since this research focuses on responses of the tree-ring data from changes of hydrological environments, 3-month, 6-month, 9-month, 12-month, 18-month, and 24-month monthly SPI are calculated in the historical period. A time-series dataset from 2003 to 2016 is extracted to compare with GRACE-DA products and tree-ring widths.

Tree Site ID	Weather Station ID	Distance (Degree)
az591	29156	0.013
az592	29156	0.013
az580	26716	0.070
ca677	48218	0.089
ca686	44997	0.163
ca687	44997	0.163
az583	26716	0.170
az585	26716	0.170
or092	357817	0.184
ms003	226009	0.185
wv006	447285	0.201
id015	101018	0.230
wv009	468614	0.257
or094	350694	0.258
nc026	319467	0.299
az596	21330	0.313
az595	21330	0.314
ca678	41072	0.318
az597	28820	0.345
az598	28820	0.345
or095	358029	0.346
or093	350501	0.351
wv007	464393	0.426
ca674	41497	0.460
ca676	40161	0.464
ca675	40161	0.474
wy046	245961	0.538
ca679	40161	0.540
ok040	348992	0.666
ok041	348992	0.666
nm589	21248	0.676
ok042	348992	0.706
wy047	486440	0.739
wy048	245080	0.787

Table 2.1: The distance between tree sites and weather stations, descending by the distance

2.1.3 Standardized Precipitation Evapotranspiration Index (SPEI)

SPEI efficiently shows the effect of evapotranspiration demand by using the difference between precipitation and potential evapotranspiration (Vicente-Serrano et al., 2010). Like SPI, SPEI is multi-scale and calculated from observation values at stations with data quality control. This study uses climate data from the same nearest weather stations to calculate the monthly SPEI data in different accumulation periods (3-month, 6-month, 9-month, 12-month, 18-month, and 24-month) from 1970 to 2016. The calculation is executed by a software developed by the NDMC. With reading historical records of precipitation, temperature, and the latitude of the weather station, the program uses the Penman-Monteith equation to obtain potential evapotranspiration (PET) and outputs monthly SPEI. The same period from 2003 to 2016 is extracted to prepare the statistical analysis.

2.1.4 Tree Ring Standardized Growth Index (TRSGI)

A tree-width index is used to quantify the accumulative biomass in a year. This study collects the Tree Ring Standardized Growth Index (TRSGI) from the International Tree-Ring Data Bank (ITRDB) which is managed by the National Oceanic and Atmospheric Administration (NOAA). TRSGI is calculated from measured tree-ring widths. First, several growth curves are developed for each tree by fitting the ring-width series to the exponential form. After an appropriate growth curve has been determined, the function is solved for the expected yearly growth (Y_t). Then, Equation (2.10) standardizes the ring-width data (W_t) by dividing each measured data by the expected annual growth, where t represents the year of each tree-ring width.

$$TRSGI = \frac{W_t}{Y_t} \quad (2.10)$$

Because of the limitation of the period of GRACE-DA products, this study is prevented

from utilizing the long historical records of TRSGI. The period of TRSGI data is from 2003 to 2010. After filtering tree-ring data in the ITRDB database by the overlapped period and quality, this study has thirty-four tree-ring sites across the contiguous U.S. Nation forest resources are divided into nine regions based on the research (Sun et al., 2015) and climatic characteristics (Figure 2.3). Twenty-six out of thirty-four trees are in the western regions: Northwest, West, West North Central, Southwest. Eight out of thirty-four sites are in Oklahoma, Mississippi, West Virginia, and North Carolina. The majority of trees (29 out of 34) are conifers. In addition, twenty-five out of thirty-four trees are over 200 years old, which indicates that some of studying trees have a good resilience of drought stress.

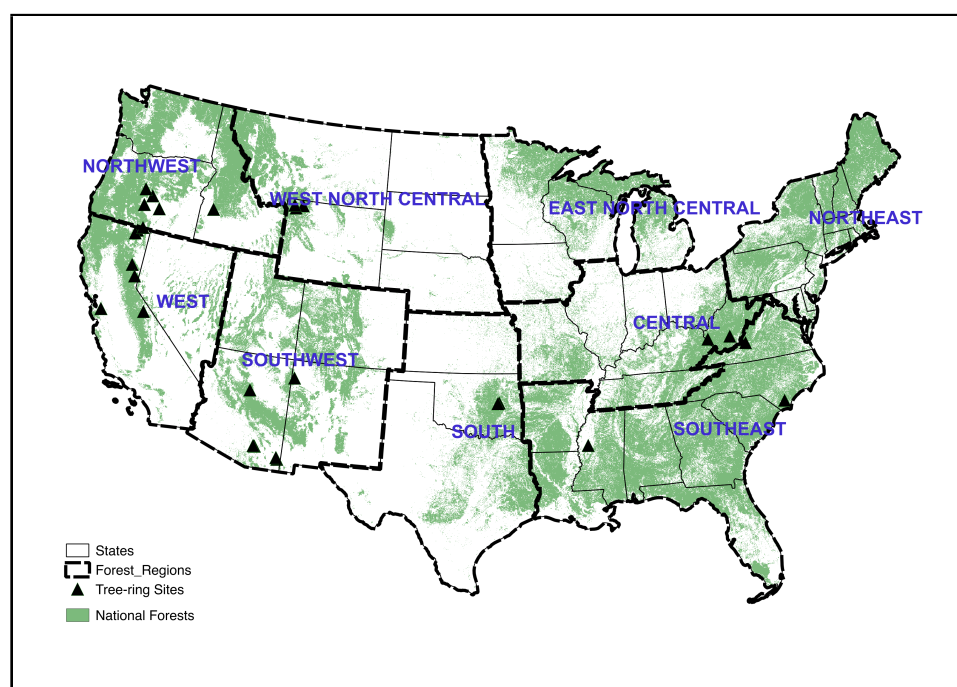


Figure 2.3: Distribution of tree-ring sites across the CONUS and the nine forest divisions: Northwest, West, West North Central, Southwest, South, East North Central, Central, Southeast, and Northeast

Table 2.2 shows the information of age and species which are collected in the TRSGI dataset with the geographic coordination (degree) and elevations (meter) on each sites location. To specify the topography of different tree sites, slopes in decimal degrees are calculated

ID	States	Species	Age
az580	Arizona	Douglas-fir	402
az583	Arizona	Douglas-fir	392
az585	Arizona	Ponderosa pine	434
az591	Arizona	Douglas-fir	365
az592	Arizona	Ponderosa pine	482
az595	Arizona	Arizona pine	180
az596	Arizona	Ponderosa pine	150
az597	Arizona	Arizona pine	149
az598	Arizona	Ponderosa pine	198
ca674	California	Ponderosa pine	560
ca675	California	Western juniper	858
ca676	California	Ponderosa pine	657
ca677	California	Jeffrey pine	595
ca678	California	Jeffrey pine	706
ca679	California	Ponderosa pine	589
ca686	California	California sycamore	310
ca687	California	Valley oak	313
id015	Idaho	Ponderosa pine	523
ms003	Mississippi	Baldcypress	772
nc026	North Carolina	Baldcypress	1645
nm589	New Mexico	Ponderosa pine	1168
ok040	Oklahoma	Shumard Oak	89
ok041	Oklahoma	Pin Oak	76
ok042	Oklahoma	Pin Oak	63
or092	Oregon	Western juniper	1480
or093	Oregon	Western juniper	1140
or094	Oregon	Western juniper	1180
or095	Oregon	Western juniper	673
wv006	West Virginia	Eastern hemlock	154
wv007	West Virginia	Eastern hemlock	256
wv009	West Virginia	Pitch pine	186
wy046	Wyoming	Engelman spruce	572
wy047	Wyoming	Lodgepole pine	252
wy048	Wyoming	Lodgepole pine	330

Table 2.2: The table describes the locations of tree sites and species and ages of trees

ID	Longitude	Latitude	Elevation	Slope	AWC	Soil Texture
az580	-109.26	31.92	2316	6.96	59	Silt Loam
az583	-109.33	32	1828	3.59	31	Silt Loam
az585	-109.33	32	1828	3.59	31	Silt Loam
az591	-111.52	35.17	2057	0.06	63	Sandy Loam
az592	-111.52	35.17	2057	0.06	63	Sandy Loam
az595	-110.71	32.41	2534	4.69	59	Sandy Loam
az596	-110.71	32.41	2534	4.69	59	Sandy Loam
az597	-110.79	32.43	2577	6.37	59	Sandy Loam
az598	-110.79	32.43	2577	6.37	59	Sandy Loam
ca674	-120.63	40.1	1385	8.68	82	Sand
ca675	-120.88	41.83	1508	3.13	89	Loam
ca676	-120.98	41.67	1513	0.43	158	Loam
ca677	-120.28	39.57	1688	4.53	99	Sandy Loam
ca678	-119.15	37.95	2499	11.17	50	Sandy Loam
ca679	-120.57	42.03	1645	6.42	120	Loam
ca686	-121.85	37.55	89	5.99	90	Loam
ca687	-121.85	37.55	89	5.99	90	Loam
id015	-116.10	43.75	1825	6.79	69	Loamy Sand
ms003	-90.50	33.27	30	0.07	270	Silty Clay Loam
nc026	-78.22	34.32	2	0.19	89	Sandy Loam
nm589	-108.87	36.09	2650	2.27	108	Sand
ok040	-95.92	35.53	188	0.19	280	Silt Loam
ok041	-95.92	35.53	186	0.19	280	Silt Loam
ok042	-96	35.5	196	0.48	72	Silt Loam
or092	-120.88	43.17	1428	1.3	123	Sandy Loam
or093	-120.47	43.7	1475	0.47	54	Loam
or094	-121.05	43.95	1146	1.06	56	Loamy Sand
or095	-119.80	43.15	1514	1.19	26	Loam
wv006	-80	37.52	670	1.68	51	Sandy Loam
wv007	-82.37	37.98	250	1.77	105	Loam
wv009	-80.93	37.97	700	1.97	132	Silt Loam
wy046	-109.90	44.73	2961	4.58	56	Loam
wy047	-110.38	44.57	2395	2.02	108	Loam
wy048	-110.50	44.7	2349	1.25	108	Loam

Table 2.3: The table describes geographic environments of tree sites which include longitude and latitude, elevation, slope, available water content (AWC), and soil texture

from the digital elevation model (DEM). Available water capacity (AWC) and soil texture are extracted respectively from Gridded Soil Survey Geographic (gSSURGO) Database and the North American Land Data Assimilation System (NLDAS). 2.3 demonstrates the additional information for investigating responses from trees in different climatic and hydrological environments.

2.1.5 Normalized Difference Vegetation Index (NDVI)

This study uses Normalized Difference Vegetation Index (NDVI) data generated by the U.S. Geological Survey's (USGS) Earth Resources Observation and Science (EROS) Center based on Moderate Resolution Imaging Spectroradiometer (eMODIS) to ascertain the growing season in each forest region. This study calculates the monthly mean NDVI of each forest region from the eMODIS NDVI masked by the national forest area from 2003 to 2017 and aggregates the NDVI values by forest regions. Founded on a prior research (Jeong et al., 2001), Equation (2.11) is used to delineate the start and the end of each growth cycle, where t is the month.

$$NDVI_{ratio}(t) = \frac{NDVI_{t+1} - NDVI_t}{NDVI_t} \quad (2.11)$$

Month	Northwest	West North Central	West	Southwest	South	East North Central	Central	Southeast	Northeast
January	0.26	-0.06	-0.03	-0.11	-0.08	-0.18	-0.07	-0.11	-0.21
February	-0.08	0.12	0.15	0.25	0.16	1.42	0.27	0.09	0.83
March	0.27	0.54	0.12	0.24	0.31	1.23	0.42	0.24	0.77
April	0.28	0.42	0.21	0.22	0.06	0.43	0.31	0.06	0.41
May	0.26	0.46	0.12	0.20	-0.02	0.29	0.08	0.02	0.20
June	0.19	0.23	0.03	-0.04	0.04	0.09	0.02	-0.03	0.03
July	-0.03	-0.06	0.01	0.07	-0.02	0.01	-0.01	0.01	0.03
August	-0.07	-0.12	-0.01	0.03	0.01	-0.11	-0.01	0.05	-0.04
September	-0.15	-0.23	-0.03	-0.11	-0.05	-0.36	-0.17	-0.04	-0.25
October	-0.38	-0.43	-0.12	-0.16	-0.18	-0.29	-0.28	-0.08	-0.21
November	-0.30	-0.36	-0.28	-0.32	-0.09	-0.63	-0.23	-0.12	-0.50
December	0.06	0.04	-0.06	-0.08	-0.05	-0.27	-0.08	-0.02	-0.23

Table 2.4: The monthly mean NDVI ratio for each national forest region

This study calculates the NDVI ratio for all forest regions (Table 2.4). Positive ratios reflect the month t when NDVI values ascend. The largest ratio represents the growing rate of leaves is the highest in the month, which can be considered as the start of the growing season in a year. Negative ratios reflect the month t when NDVI values descend. The smallest ratio represents the deciduous stage in a year, which can be considered as the end of the growing season. Since the annual growth of trees exhibit systematic changes in the tree-ring width (Fritts, 2012), this study determines the period from March to October as the forest growing season based on the $NDVI_{ratio}$, which is used to compare with different tree sites across the CONUS.

2.2 Statistical Methods

2.2.1 Simple Linear Correlation

The Pearson correlation is calculated between two dataset pairs including: (1) z-score monthly GWS anomalies and SPI (3, 6, 9, 12, 18, 24 months); (2) z-score monthly GWS anomalies and SPEI (3, 6, 9, 12, 18, 24 months); (3) z-score monthly RZSM anomalies and SPI; and (4) z-score monthly RZSM anomalies and SPEI. The Pearson correlation coefficient determines the strength of the association between two variables. This method has two assumptions for the pairs of datasets being compared: (1) they are independent; and (2) they follow a normal distribution. Positive Pearson correlation coefficients indicate that both variables have similar increasing or decreasing trends, whereas negative coefficients indicate that the two variables have an opposite linear trend. The higher positive values and lower negative values indicate stronger relationships between the two datasets.

$$r = \frac{\sum_{i=1}^n (x_i - \bar{x})(y_i - \bar{y})}{\sqrt{\sum_{i=1}^n (x_i - \bar{x})^2 (y_i - \bar{y})^2}} \quad (2.12)$$

In this study, the comparisons of GRACE information and drought indicators (SPI and SPEI) in different accumulation periods not only indicate the time lags between the anomalies of subsurface water storage (GWS and RZSM) and the changes of precipitation and evapotranspiration, but also are useful to understand the different accumulative effects on tree growth from precipitation, groundwater, and soil moisture.

2.2.2 Bootstrapping

To investigate the relationships between the yearly dataset (TRSGI) and the monthly datasets (z-score monthly GWS anomalies, z-score monthly RZSM anomalies, SPI, and SPEI), a bootstrapping method is utilized to estimate the statistical distribution of the population by randomly sampling 1000 times with replacement. After estimating the distribution for all variables, Pearson correlation coefficients are calculated between the TRSGI and monthly GWS anomalies, monthly RZSM anomalies, SPI (3, 6, 9, 12, 18, 24 months), and SPEI (3, 6, 9, 12, 18, 24 months). Since the TRSGI has already captured the effect of previous year conditions, the correlation coefficients were calculated only for months of ring formation (March to October). The results of bootstrapping Pearson correlation involve all correlation coefficients that are calculated by month in the growing season for the nine forest regions. The correlation values of tree sites in each area are averaged for analyzing the spatial effects. The confidence intervals are set to confine the significant level of 0.05. The results indicate the different impacts of GWS, RZSM, SPI, and SPEI on the tree-ring growth in different months through a year and quantify the relationships among the TRSGI and all other variables.

2.2.3 Multiple Linear Regression

Multiple linear regression is used to evaluate the relative contribution for each component and develop a predictive model for the dependent variable. This study proposes and diagnoses

multiple linear regression models to investigate the relationships between TRSGI and the changes of GWS and RZSM anomalies with combined impacts of SPI and SPEI. The full model is proposed as the Equation (2.13) to explore whether linear relationships between TRSGI and a subset or all of SPI, SPEI, z-score monthly GWS, and RZSM anomalies. By using the exhaustive algorithm in the `regsubsets` function of the R package `leaps`, this study develops three possible reduced models (Equation (2.14), (2.15), (2.16)), investigating and quantifying respective relationships between tree-ring growth and subsurface water anomalies (z-score monthly GWS and RZSM anomalies). The reduced Model (2.12) illustrates the relationships between tree-ring width and RZSM anomalies. Model (2.13) considers influences of SPEI. And based on the Model (2.13), the Model (2.14) adds impacts of GWS anomalies. These reduced models are used to compare with the Model (2.15) and test if the GWS or RZSM has the capability to predict the growth of trees. In this study, 2/3 of datasets are used to build models and the remaining 1/3 of the data are used to test the models. For all models, the null hypothesis is that all slope coefficients are equal to zero, and the alternative hypothesis is at least some of slope coefficients are not equal to zero. β_1 , β_2 , β_3 , and β_4 represent different slope coefficients in different models, where β_0 is the interception coefficient and ϵ is the independent normal random variable with mean zero and a constant variance.

$$TRSGI = \beta_0 + \beta_1 RZSM + \epsilon \quad (2.13)$$

$$TRSGI = \beta_0 + \beta_1 SPEI + \beta_2 RZSM + \epsilon \quad (2.14)$$

$$TRSGI = \beta_0 + \beta_1 SPEI + \beta_2 GWS + \beta_3 RZSM + \epsilon \quad (2.15)$$

$$TRSGI = \beta_0 + \beta_1 SPI + \beta_2 SPEI + \beta_3 GWS + \beta_4 RZSM + \epsilon \quad (2.16)$$

This study calculates the adjusted R-Squared, the Akaike's information criterion (AIC), the corrected AIC, and the Bayesian information criterion (BIC) to evaluate the goodness of fit of the full model and reduced models. A higher value of adjusted R-Squared or lower values of AIC and BIC represent the estimated model with a better fitting capability. Mean squared prediction error (MSPE), min-max accuracy, and mean absolute percentage error (MAPE) are calculated on the testing datasets as forms of predictive accuracy measure. Lower MSPE and MAPE and higher min-max accuracy imply that the observed and predicted values are closer and the predictability is better. Based on the observations of the thirty-four study sites, drought indices (SPI, SPEI), and GRACE-DA derived outputs (monthly GWS and RZSM anomalies), this study will investigate the impacts of subsurface water storage anomalies on tree-ring widths by training and testing multiple linear regression models.

Chapter 3

Results and Discussion

3.1 Correlation between monthly GWS anomalies and drought indices (SPI and SPEI)

This study calculates the Pearson correlation coefficients between the z-score GWS monthly anomalies and the 3-month, 6-month, 9-month, 12-month, 18-month, and 24-month SPI and SPEI values at the tree-ring sites. While the z-score GWS monthly anomalies are computed as standard deviations of the subsurface water volume below 1 meter and drought indices are accumulated over different time periods, the correlation values provide valuable comparisons of variables at different time scales and responses from monthly GWS anomalies when there is a drought.

Figure 3.1 is a boxplot of comparisons of SPI and monthly GWS anomalies at different time scales. Mean, median, minimum, and maximum values are listed in Table 3.1. The correlation increases when the cumulative period becomes longer among the 34 sites, peaking at the 12-month SPI. In the comparison of SPI3, most correlation values are much lower between 0.18 and 0.4 and with the mean value of 0.29. Correlation coefficients rise significantly when the time scale increases to 6 months or longer. Most of the tree sites have relatively stronger correlations, and the average value is 0.395. The correlations increase steadily throughout the accumulation periods. SPI12 has the strongest relationship with

GWS anomalies with a mean value of 0.45 and a median value of 0.47. The results for the SPI18 and SPI24 are very similar to SPI 12 with slightly lower mean and median correlation coefficients. The overall trend of these comparisons also indicates the time lag between precipitation anomalies and GWS anomalies could be extended to 24 months in some regions. However, the correlation coefficients in the same comparison have large spatial variations. For example for SPI12, although over half of comparisons are over 0.47, the minimum value is still negative. The negative correlation coefficients appear among different accumulation periods, and they are highly similar at the spatial scale.

	Mean	Median	Minimum	Maximum
GWS-SPI3	0.29	0.28	-0.10	0.65
GWS-SPI6	0.40	0.44	-0.14	0.74
GWS-SPI9	0.44	0.46	-0.11	0.79
GWS-SPI12	0.45	0.47	-0.08	0.80
GWS-SPI18	0.43	0.46	-0.11	0.75
GWS-SPI24	0.44	0.46	-0.05	0.79

Table 3.1: The mean, median, minimum, and maximum of correlation coefficients between GWS anomalies and SPI in 3-month, 6-month, 9-month, 12-month, 18-month, 24-month accumulation periods for the 34 tree-ring sites

The correlations between monthly GWS anomalies and SPEI have the same homogeneity as SPI through different accumulation periods. As displayed in Table 3.2, the relationship becomes relatively stronger as the cumulative time increases. The comparison of SPEI12 and GWS anomalies has the highest correlation coefficient on the average of 0.53. The correlation between SPEI and GWS also significantly increases when the accumulation period extends from 3 months to 6 months. After the peak, the mean values of correlations are fairly steady at 0.5. However, the median correlation coefficients decline to 0.46 and 0.48 over twelve months, respectively. Figure 3.2 indicates the correlation coefficients also have a large variance in the same comparison.

Overall, the trend of the comparisons between SPI and monthly groundwater anomalies

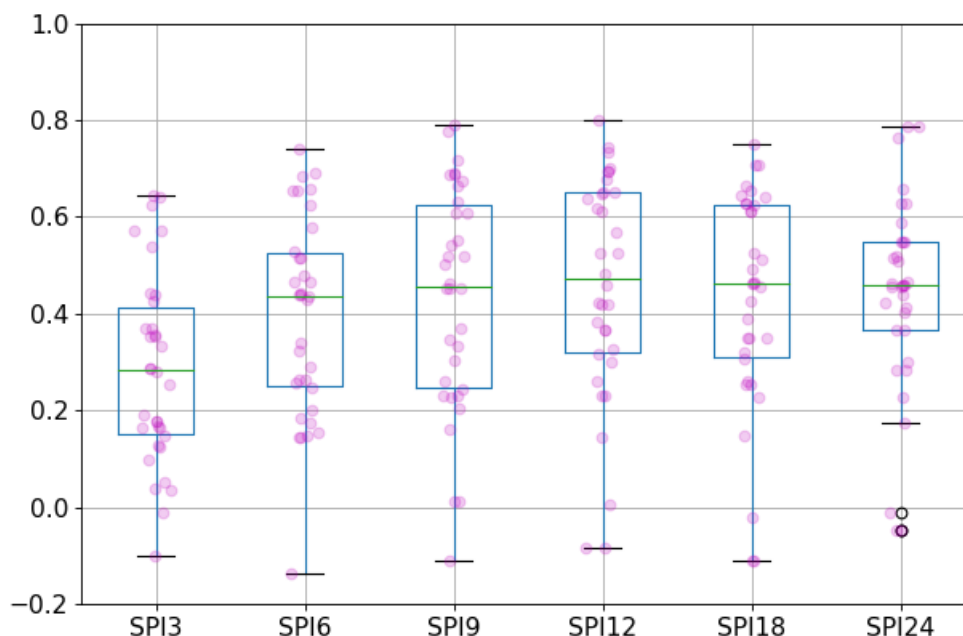


Figure 3.1: Boxplot of correlation coefficients between GWS anomalies and SPI in 3-month, 6-month, 9-month, 12-month, 18-month, 24-month accumulation periods for the 34 tree-ring sites, where the black circles show the outliers

is similar to the comparisons between SPEI and monthly groundwater anomalies. Adding the effect of evapotranspiration in the calculation make the correlations of SPEI slightly higher than the precipitation-based SPI. The Comparisons indicate both SPI and SPEI have the strongest correlations with GWS anomalies when the accumulation period is 12 months. The correlation coefficients vary greatly at different study sites.

Figure 3.3 shows the spatial patterns of correlations between SPI in different accumulation periods and GWS anomalies at each site. All comparisons have similar spatial patterns across the different periods analyzed. The sites have stronger relationships in California, Oklahoma, West Virginia, Mississippi, and North Carolina. The correlation coefficients of SPI are lower in Oregon, Idaho, New Mexico, and some areas of Arizona

	Mean	Median	Minimum	Maximum
GWS-SPEI3	0.34	0.32	0.03	0.66
GWS-SPEI6	0.46	0.45	0.04	0.76
GWS-SPEI9	0.50	0.49	0.06	0.82
GWS-SPEI12	0.53	0.53	0.15	0.83
GWS-SPEI18	0.51	0.46	0.09	0.81
GWS-SPEI24	0.50	0.48	0.05	0.85

Table 3.2: The mean, median, minimum, and maximum of correlation coefficients between GWS anomalies and SPEI in 3-month, 6-month, 9-month, 12-month, 18-month, 24-month accumulation periods for the 34 tree-ring sites

because of the geological and climatic environment. The Pacific Northwest basaltic-rock aquifers are under the sites in Oregon and Idaho. These igneous rocks can only be infiltrated where they are cracked, which would suggest that precipitation has very slow influences on groundwater recharge. Except for tree sites or092 and nm589, the remaining sites in Oregon and Idaho have increasing correlations with the cumulative period being longer. In the south of Arizona, the semi-arid hot climate determines that the evaporation becomes very crucial for the water circulation. Lower correlations between SPI and monthly GWS anomalies are rational at sites in the south of Arizona because the precipitation-based SPI omits the effects of evaporation. The negative values are only found at three sites: az597, az598, and or092 through all accumulation periods, and the az597 and the az598 have the same geographic coordination. And the correlation coefficients at these sites remain around zero for all accumulation periods. Time-series graphs of monthly GWS anomalies and SPI at these sites are presented in Appendix I. Changes of local land use and land cover and the quality of monthly GWS anomalies might be reasons why there are significant discrepancies at these locations. But further studies need to be developed in these regions.

All sites have positive correlations between monthly GWS anomalies and SPEI in all accumulation periods (Figure 3.4). The correlation maps of SPEI have similar spatial patterns to the SPI. Sites in central parts of California, Oklahoma, West Virginia, Mississippi,

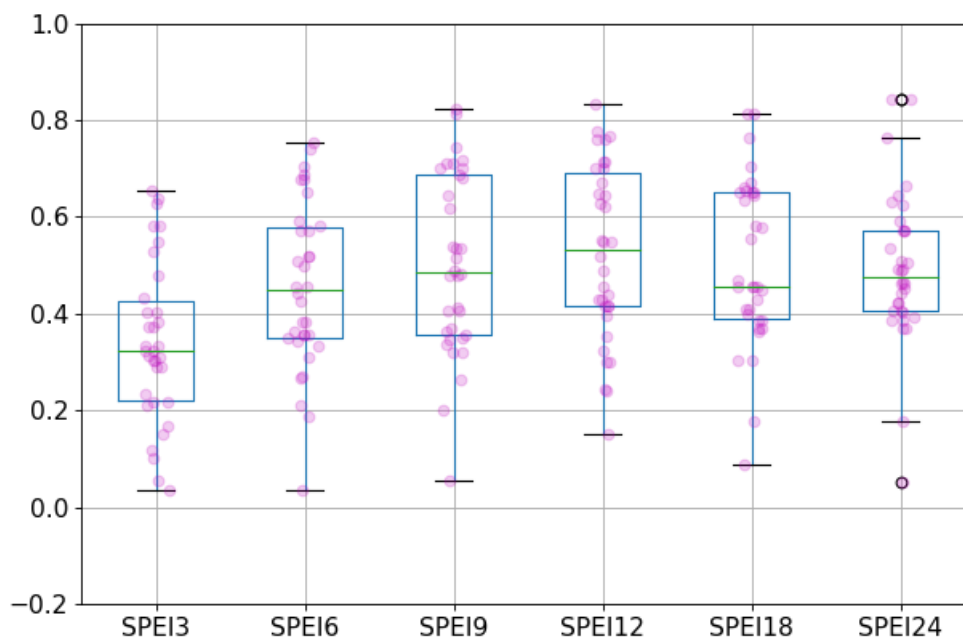


Figure 3.2: Boxplot of correlation coefficients between GWS anomalies and SPEI in 3-month, 6-month, 9-month, 12-month, 18-month, 24-month accumulation periods for the 34 tree-ring sites, where the black circles show the outliers

and North Carolina have a strong correlation between SPEI12 and GWS (0.63 - 0.83). By considering the component of evapotranspiration through the addition of temperature in the circulation, the long-term SPEI has a higher correlation with GWS in semi-arid areas such as Arizona. However, the correlation in New Mexico is still at a relatively low value (0.05 - 0.34). The correlation at the site or094 increases substantially when the accumulation period expands from 3 months to 12 months (0.31 - 0.62), whereas the other sites in Oregon have relatively lower coefficients at 12 months (0.18 - 0.40). Since the climatic and geological environments are similar between upper California and Oregon, the comparisons at sites (ca675, ca676, ca679) resemble sites in Oregon. Similar to the SPI, the correlation coefficients of SPEI18 and SPEI24 decrease slightly in New Mexico, Oklahoma, and West

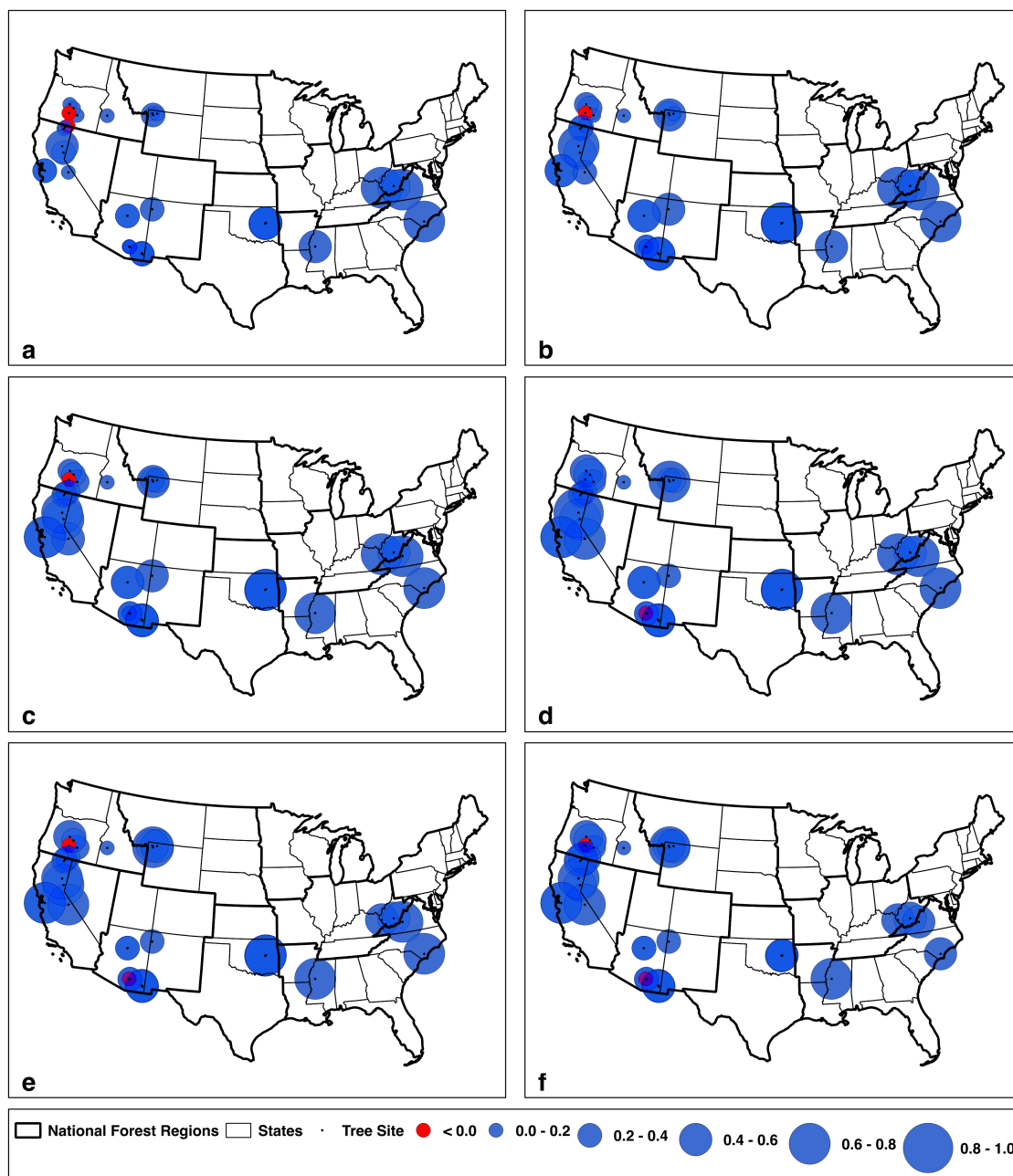


Figure 3.3: Maps showing the spatial patterns of correlations between GWS anomalies and SPI at 34 sites. The radius of the symbol represents the correlation coefficient. A larger circle stands for a higher correlation. (a) GWS-SPI3, (b) GWS-SPI6, (c) GWS-SPI9, (d) GWS-SPI12, (e) GWS-SPI18, (f) GWS-SPI24



Figure 3.4: Maps showing the spatial patterns of correlations between GWS anomalies and SPEI at 34 sites. The radius of the symbol represents the correlation coefficient. A larger circle stands for a higher correlation. (a) GWS-SPEI3, (b) GWS-SPEI6, (c) GWS-SPEI9, (d) GWS-SPEI12, (e) GWS-SPEI18, (f) GWS-SPEI24

Virginia.

Generally, monthly GWS anomalies have strong relationships with both the long-term SPI and SPEI in central California, Wyoming, Oklahoma, West Virginia, Mississippi, and North Carolina. However, GWS anomalies have fewer connections with either SPI or SPEI in New Mexico. In upper California, Oregon, Idaho, and Arizona, the long-term SPEI has a better correlation with GWS anomalies than the SPI.

3.2 Correlation between monthly RZSM anomalies and drought indices (SPI, SPEI)

Monthly RZSM anomalies reflect the changes of soil moisture within the top 1 meter of soil. Being compared with GWS anomalies, RZSM anomalies have quicker responses to drought conditions. It is a primary driver for water stress on vegetation. This study calculates Pearson correlations between monthly RZSM anomalies and different accumulation periods of SPI and SPEI (3-month, 6-month, 9-month, 12-month, 18-month, and 24-month). The correlation coefficients indicate the impacts of varying accumulation periods on RZSM and investigate the reaction of monthly RZSM anomalies on droughts.

Table 3.3 and Figure 3.5 indicate that monthly RZSM anomalies have the highest correlation with SPI3. With the accumulation period increasing from 3 months to 24 months, the average correlation coefficients between monthly RZSM anomalies and SPI decreases from 0.53 to 0.38. Although the median correlation with SPI6 (0.53) is higher than SPI3 (0.52), the correlation of SPI3 has the smallest variance. When the time is accumulated over nine months, the correlation coefficients continue reducing, and the variances increase. Figure 3.6 demonstrates the spatial patterns of correlations across various accumulation times. The correlation coefficients stay at a low level at sites ca678, id015, wy046, and wy048. Aside from these locations, the remainder of the sites shows stronger correlations in

the comparison of RZSM anomalies and SPI3.

	Mean	Median	Minimum	Maximum
RZSM-SPI3	0.53	0.52	0.28	0.67
RZSM-SPI6	0.49	0.53	0.17	0.75
RZSM-SPI9	0.47	0.48	0.06	0.76
RZSM-SPI12	0.45	0.43	0.06	0.76
RZSM-SPI18	0.41	0.39	0.06	0.72
RZSM-SPI24	0.38	0.39	0.09	0.76

Table 3.3: The mean, median, minimum, and maximum of correlation coefficients between RZSM anomalies and SPI in 3-month, 6-month, 9-month, 12-month, 18-month, 24-month accumulation periods for the 34 tree-ring sites

The correlations between RZSM and multiple temporal-scale SPEI also decrease with accumulation periods increasing. The SPEI exhibits, on average, a relatively stronger relationship with RZSM anomalies than SPI among the 34 study sites. As shown in Table 3.4, SPEI3 has the strongest relationship with RZSM anomalies. The mean of RZSM-SPEI3 is 0.56 and the median is 0.58. In Figure 3.7, the correlation values of SPEI3 has the smallest variance among the comparisons between RZSM anomalies and SPEI. The average correlation coefficients reduce from 0.53 to 0.40 when the accumulation periods increase from 6 months to 24 months.

Figure 3.8 displays the comparisons of RZSM anomalies and SPEI for different accumulation periods in the U.S. The spatial patterns of the correlation between RZSM anomalies and SPEI resemble those for the SPI. Although the impacts of evapotranspiration on improving the correlations in the comparisons of RZSM anomalies are not as significant as the comparisons of GWS anomalies, the most of stations still have a slightly stronger relationship between RZSM anomalies and SPEI3 than the SPI3 except for sites ca678, or092, wy046, and wy048. As the accumulation time expanded, the correlation coefficients at most sites also decrease.

However, the comparisons at sites in central California (ca674, ca677, ca678, ca686,

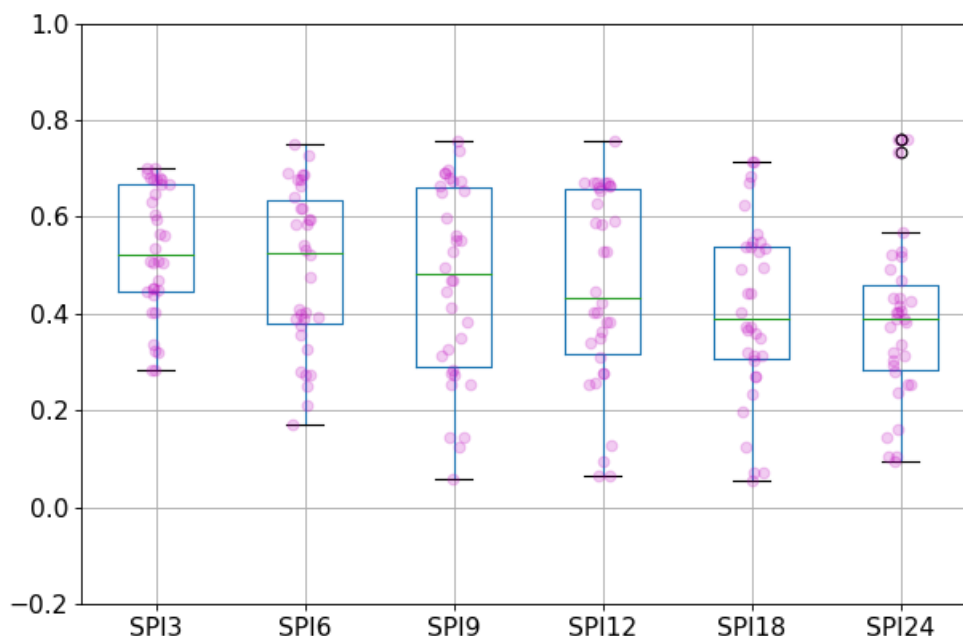


Figure 3.5: Boxplot of correlation coefficients between RZSM anomalies and SPI in 3-month, 6-month, 9-month, 12-month, 18-month, 24-month accumulation periods for the 34 tree-ring sites, where the black circles show the outliers

ca687) have a contrary trend that the correlations between RZSM anomalies and two indices (SPI, SPEI) are increasing as accumulation periods increased. The site ca678 has the most significant increase and peaks at SPI24/SPEI24 compared to the other sites. The remainder of sites have the highest correlation coefficients in the comparisons of SPI9 and SPEI9. The time-series graphs at these sites show that the oscillation of RZSM anomalies is smaller than other locations. Since the long-term SPI and SPEI have a smoother linear trend, the correlation coefficients are increasing as the accumulation period increased. This result may be caused by the changes in land use and the geophysical environment. For example, sites ca674, ca677, and ca678 are located at the eastern side of the Sierra Nevada Mountain where there is a semi-arid climate. The soil moisture might be relatively constant over a long



Figure 3.6: Maps showing the spatial patterns of correlations between RZSM anomalies and SPI at 34 sites. The radius of the symbol represents the correlation coefficient. A larger circle stands for a higher correlation. (a) RZSM-SPI3, (b) RZSM-SPI6, (c) RZSM-SPI9, (d) RZSM-SPI12, (e) RZSM-SPI18, (f) RZSM-SPI24

	Mean	Median	Minimum	Maximum
RZSM-SPEI3	0.56	0.58	0.31	0.72
RZSM-SPEI6	0.53	0.53	0.26	0.79
RZSM-SPEI9	0.50	0.48	0.12	0.79
RZSM-SPEI12	0.49	0.50	0.15	0.77
RZSM-SPEI18	0.43	0.41	0.12	0.79
RZSM-SPEI24	0.40	0.38	0.10	0.80

Table 3.4: The mean, median, minimum, and maximum of correlation coefficients between RSZM anomalies and SPEI in 3-month, 6-month, 9-month, 12-month, 18-month, 24-month accumulation periods for the 34 tree-ring sites

period. However, further studies are required to investigate a possible relationship between the 1-meter soil moisture anomalies and accumulative precipitation in California.

3.3 Comparison between monthly GWS anomalies and TRSGI

Tree Ring Standardized Growth Index (TRSGI) was developed to interpret the effects of environmental signals in the tree-growth period ("Tree Ring Data Description", n.d.). The comparison between monthly GWS anomalies and TRSGI is valuable to understand the impacts of changes of subsurface water storage under 1-meter depth on the tree growth. This study uses the bootstrapping method to resample the TRSGI dataset and calculates the Pearson correlation coefficient between TRSGI and GWS anomalies by month in the growing season (March to October). Different correlation coefficients in the growing season indicate the same environmental variable has a different extent of impacts on tree-ring growth.

The heatmap (Figure 3.9) presents the mean Pearson correlations between monthly GWS anomalies and resampled TRSGI for the ten states where the study sites are located. In North Carolina, New Mexico, Oregon, and Wyoming, the average of correlation coefficients within the state is insignificant during the entire growing season. The aquifer under the sites in Oregon is a carbonate-rock aquifer, which makes groundwater hard to discharge and

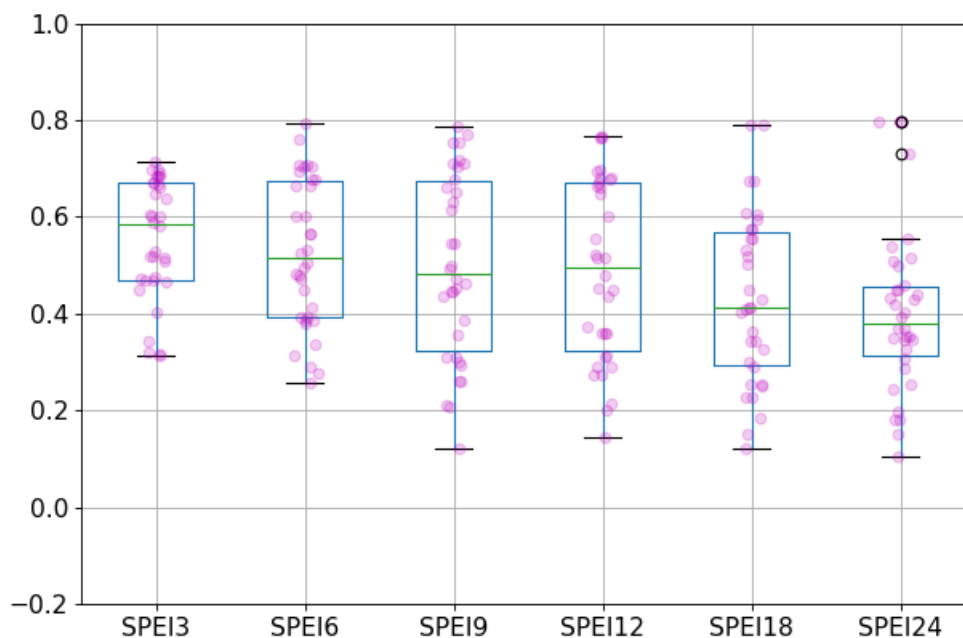


Figure 3.7: Boxplot of correlation coefficients between RZSM anomalies and SPEI in 3-month, 6-month, 9-month, 12-month, 18-month, 24-month accumulation periods for the 34 tree-ring sites, where the black circles show the outliers

recharge. The changes in groundwater do not have significant effects on tree growth. In addition, this study also calculates the mean Pearson correlation between resampled TRSGI and SPI/SPEI in different accumulation periods (see Appendix II). Both SPI and SPEI are significantly correlated to TRSGI at the sites in Oregon. For the sites in Wyoming, there is no considerable correlation between TRSGI and GWS anomalies, SPI, and SPEI. The tree site in North Carolina has only one significant correlation between SPI12 and TRSGI. The tree site in New Mexico (nm589) has significant comparisons of SPEI3, SPEI6, and SPI3. In the previous results of the correlations between monthly GWS anomalies and drought indicators (SPI and SPEI), the correlation value peaks at SPI9 and SPEI6 at the nm589, respectively. A possible reason is that the local water table is relatively shallow and the



Figure 3.8: Maps showing the spatial patterns of correlations between RZSM anomalies and SPEI at 34 sites. The radius of the symbol represents the correlation coefficient. A larger circle stands for a higher correlation. (a) RZSM-SPEI3, (b) RZSM-SPEI6, (c) RZSM-SPEI9, (d) RZSM-SPEI12, (e) RZSM-SPEI18, (f) RZSM-SPEI24

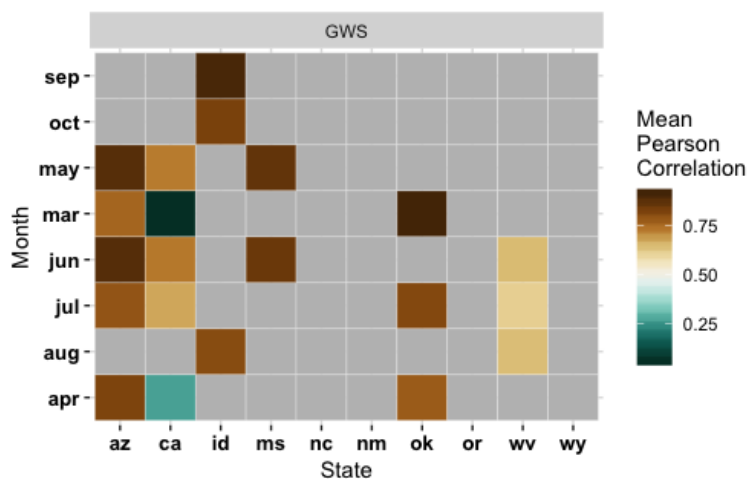


Figure 3.9: The heatmap showing the correlations between month GWS anomalies and resampled TRSGI in ten states, where grey represents insignificant correlations, and brown represents high correlations and black represents low correlations.

formation of the local aquifer is the sandstone. Deep moisture and groundwater have quicker responses to precipitation. Thus, the growth of trees would have significant correlations with SPI3, SPEI3, and SPEI6. However, further studies still need to be conducted in the local area for a larger number of study sites. Additionally, except for the site in North Carolina, the other insignificant sites have relatively low correlation coefficients between GWS anomalies and SPI and SPEI. In the future, additional studies are required to explore possible reasons why relationships between tree-ring growth and environmental variables are weak in these regions.

As shown in Figure 3.9, the means of correlations at the sites in Arizona, California, Idaho, Mississippi, Oklahoma, and West Virginia are significant during the growing season. In Arizona, 33% of sites (az580, az583, az586) have significant correlations between GWS anomalies. These tree sites are all located in the southeastern mountains areas of Arizona. The GWS anomalies in June have the most significant correlation with TRSGI at these locations, followed by May and July. There are 37.5% of tree sites (ca674, ca675, ca676) that are significantly correlated with GWS anomalies in California. However, the site ca675

that is located on the western slope of Blue Mountain has significantly negative coefficients in March and April. Overall, the GWS anomalies in June have a major role in the tree-ring growth in California. In Idaho, there is only one tree-ring site, and the correlation between GWS anomalies and TRSGI is the most significant in September. This study suggests that snowmelt which slowly recharges to deep soil moisture and groundwater and its accumulative effects could have a notable contribution to the growth of tree rings at these study sites and explain why the late growing season has the strongest correlation. In May, the GWS anomalies have the most significant impact on the TRSGI at the site ms003 in Mississippi. Generally, GWS anomalies in March have the most significant impact on tree-ring growth at all of the tree sites (ok040, ok041, ok042) in Oklahoma. One of three sites (wv007) in West Virginia has a significant correlation in June.

Since the TRSGI dataset is extracted based on the overlapping period of variables, the species of trees are mixed among the sites with significant correlations. Different species have different drought tolerances and chronology characteristics. This creates additional variations when this study compares the consequences of the monthly GWS anomalies on the tree-ring growth in different locations. In general, twelve of thirty-four sites have significant relationships between GWS anomalies and TRSGI. The results of comparisons in California, Idaho, and Oregon suggests that the geological environments, such as the depth of the water table and the formation of the local aquifer and the climatic region, play crucial roles in the relationship. The correlations in northern California and southeastern Arizona also suggest that a tree grows on the unconsolidated and semi-consolidated sand and gravel aquifers with a relatively higher water table tend to have a strong relationship between GWS anomalies and TRSGI in the early or late growing season. Although snowmelt also has a considerable impact on tree-ring growth in the mountains areas, the water that enters groundwater from excessive snowmelt will result in a large increase of the water table and have a negative influence on the tree-ring growth in the growing season.

3.4 Comparison between monthly RZSM anomalies and TRSGI

This study also investigates the impacts of root zone soil moisture on tree-ring growth. In comparison to GWS anomalies, the monthly RZSM anomalies indicate more rapid variations of water in the 1-meter-depth soil layer. For the areas with a deep water table or a relatively impermeable aquifer, such as Oregon and Idaho, the RZSM anomalies might have a larger impact on tree growth than the GWS anomalies. Like the comparison of the monthly GWS anomalies, this study calculates the mean of Pearson correlation coefficients between the monthly RZSM anomalies and the resampled TRSGI by bootstrapping in each state through the growing season. A higher absolute value of the correlation coefficient represents a stronger positive or negative relationship between RZSM anomalies and resampled TRSGI in a month of the growing season.

Figure 3.10 demonstrates the average correlation coefficients between monthly RZSM anomalies and resampled TRSGI. The x-axis is the state where the sites are in, and the y-axis is the month in the growing season. The sites in New Mexico and Wyoming are still not significant in the comparison of RZSM anomalies. It matches the result in section 3.4 that the tree-ring width is not directly related to environmental variables. This study suggests that the different biological performances of trees in a drought event could be one of the possible reasons. Trees can be grouped into two types: isohydric and anisohydric, based on different reactions in the soil water stress. Isohydric plants will close the stomata to maintain the daily leaf water potential at a constant level when the soil moisture is decreasing. The daily leaf water potential of the anisohydric plants will fall when the soil moisture is reducing. Therefore, the potential of observing a drought event in the tree-ring record of an isohydric tree is higher than an anisohydric tree. This characteristic is not defined by species. On the contrary, there are few species that correspond exactly to definitions of isohydric or anisohydric (Hochberg et al., 2018). Since the local environments are various

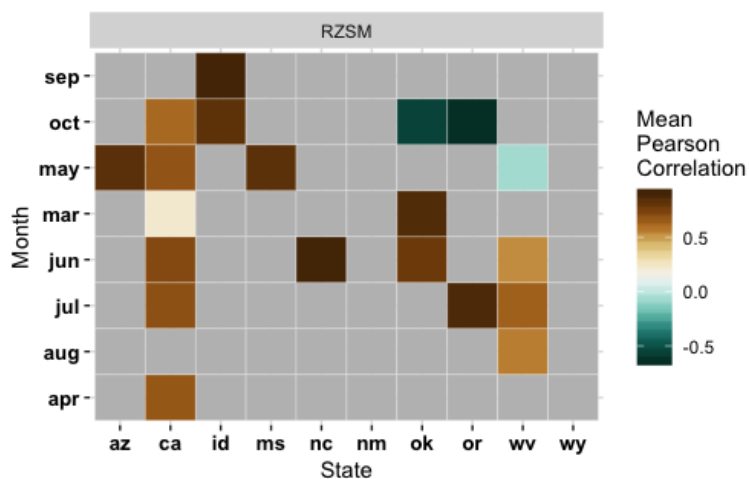


Figure 3.10: The heatmap showing the correlations between month RZSM anomalies and resampled TRSGI in ten states, where grey represents insignificant correlations, brown and black represents high positive and negative correlations respectively, and brighter color represents lower correlation

and tree species are mixed in Wyoming and New Mexico, the trees in these regions might be anisohydric (E. North, personal communication, June 23, 2019). However, this research cannot exclude the effects of geographic and geological environments. Further studies are needed to compare a larger number of TRSGI datasets with longer historical records of climatic data in the same areas.

In Arizona, California, Idaho, Mississippi, North Carolina, Oklahoma, Oregon, and West Virginia, correlations between the monthly RZSM anomalies and TRSGI are significant in the growing season. RZSM anomalies in May have the largest correlation with TRSGI in Arizona. The sites with significant correlations (az580, az583, az586) are the same as the sites in comparison of GWS anomalies. 75% of sites in California have significant correlations in different months of the growing season. Similar to the comparison of GWS anomalies and the TRSGI at the site ca675, a significantly negative relationship is observed between RZSM anomalies and the TRSGI at the same study site in March. These results suggest that the tree-ring widths decrease as the values of GWS or RZSM anomalies

increase at the study site. Based on the local climatic and geographic environments, this study suggests that the drier conditions in March and April indicate that less snowpack is accumulated during the winter and the early spring is relatively warm. In the same way, if the values of GWS and RZSM anomalies are higher in March and April, there would be a larger volume of snowpack during the winter, and the temperature in the early spring would be relatively lower. Therefore, this study suggests the growth of a tree might be delayed due to the low temperature in the early spring if the values of GWS and RZSM anomalies are higher in March and April in the Blue Mountain areas (M. Hayes, personal communication, July 31, 2019). However, since the ca675 is the only study site in the Blue Mountain areas, it is hard to conclude a certain reason for this interesting observation. In order to investigate the impact of local geographic environments and improve the reliability of results, further studies need to be conducted with a larger number of study sites on the western slope of Blue Mountain. Generally, the average correlation coefficients in California reach a peak in May. The site id015 in Idaho has the strongest relationship between the RZSM anomalies and TRSGI in September. For the site in Mississippi, the root zone soil moisture in May has the most considerable impact on tree-ring width in the same year. In Oregon where the precipitation can hardly recharge into the groundwater, the correlations between the RZSM anomalies and TRSGI are significantly higher than the comparisons of GWS anomalies, which matches to this study's prospects. The sites in Oregon have the most significant correlations, on average, in July. For the site in North Carolina, RZSM anomalies in June are significantly correlated with TRSGI. The sites in Oklahoma have the most considerable mean of correlation coefficients in March. For the sites in West Virginia, in general, the RZSM anomalies are significantly correlated with TRSGI in July.

Overall, monthly RZSM anomalies have a stronger relationship with TRSGI as compared with monthly GWS anomalies. Twenty out of the thirty-four sites have a significant correlation between RZSM anomalies and TRSGI during the growing season in

this study. The correlation also highly depends on local geological and climatic environments. For example, the site ca678 in California is located at the steep eastern slope of the Mono Dome where the soil moisture has a larger impact on the tree growth in the growing season. And the site ca677 with the same geographic environment has similar correlation coefficients in the growing season as compared to the site ca678. Although different species of trees and geographic environments cause larger variations in comparisons, monthly RZSM anomalies in the early and late growing season generally reflect the growth of trees in a year in locations where the soil moisture has a significant influence on the tree-ring width.

3.5 Multiple linear regression analysis

Section 3.3 and 3.4 demonstrate that GWS anomalies and RZSM anomalies in the growing season have a significant relationship with the tree-ring width in some areas. And the previous study shows that the SPI and SPEI in a longer accumulation period have strong relationships with tree-ring width (Bhuyan et al., 2017). This study also calculates the correlation coefficients between TRSGI and SPI and SPEI in all accumulation periods (see Appendix II). Based on the results, this study selects the sites in California, Arizona, Oklahoma, and Mississippi to develop and test multiple linear regression models and investigate the effects of months GWS or RZSM anomalies on predicting the tree-ring widths. The SPI9, SPEI9, monthly GWS anomalies, and monthly RZSM anomalies are used as predictor variables, while the TRSGI is the dependent variable. Based on the correlation coefficients between environmental variables and resampled TRSGI, this study chooses predictor variables in different months to present yearly influences in different locations (Table 3.5).

Figure 3.11 is a scatterplot that demonstrates relationships between each of the two variables. It indicates good linearities in two sets of predictors: SPI and SPEI, GWS

	SPI	SPEI	GWS	RZSM
Arizona	July	May	May	June
California	March	April	May	June
Mississippi	May	May	May	May
Oklahoma	March	March	March	March

Table 3.5: The mean, median, minimum, and maximum of correlation coefficients between RSZM anomalies and SPEI in 3-month, 6-month, 9-month, 12-month, 18-month, 24-month accumulation periods

anomalies and RZSM anomalies. Since both SPI and SPEI are defined by accumulated precipitation, and GWS is calculated from an equation of RZSM, it is rational to have these strong linear relationships. Moreover, based on the result in section 3.1 and 3.2, the average Pearson correlation coefficients between SPI9, SPEI9 and GWS anomalies, RZSM anomalies are from 0.4 to 0.5. In Figure 3.11, it shows a slightly positive trend in the relationship of SPI-GWS, SPI-RZSM, SPEI-GWS, SPEI-RZSM.

3.5.1 Variable Selection

This study uses the `regsubsets` function in the R package `leaps` to calculate the best subset from one predictor variable to four predictor variables. The `regsubsets` uses the exhaustive selection function to filter the result (Table 3.6). For the linear regression with one predictor variable, RZSM anomalies are the best option. And the combination of SPEI and RZSM anomalies is the best in two-predictor regressions. The linear regression that includes SPEI, GWS anomalies, and RZSM anomalies is the best compound of three subsets.

In order to define the best linear regression model, the adjusted R square, AIC, AICc, BIC, and PRESS are calculated for all possible subsets in this study. Table b demonstrates the values of these criteria in each model. As indicated in Table 3.6, except for the BIC, the rest of the criteria all suggest the model with two subsets could be the best model. Therefore, this study proposes the linear regression model (Equation (2.14)) to fit and predict

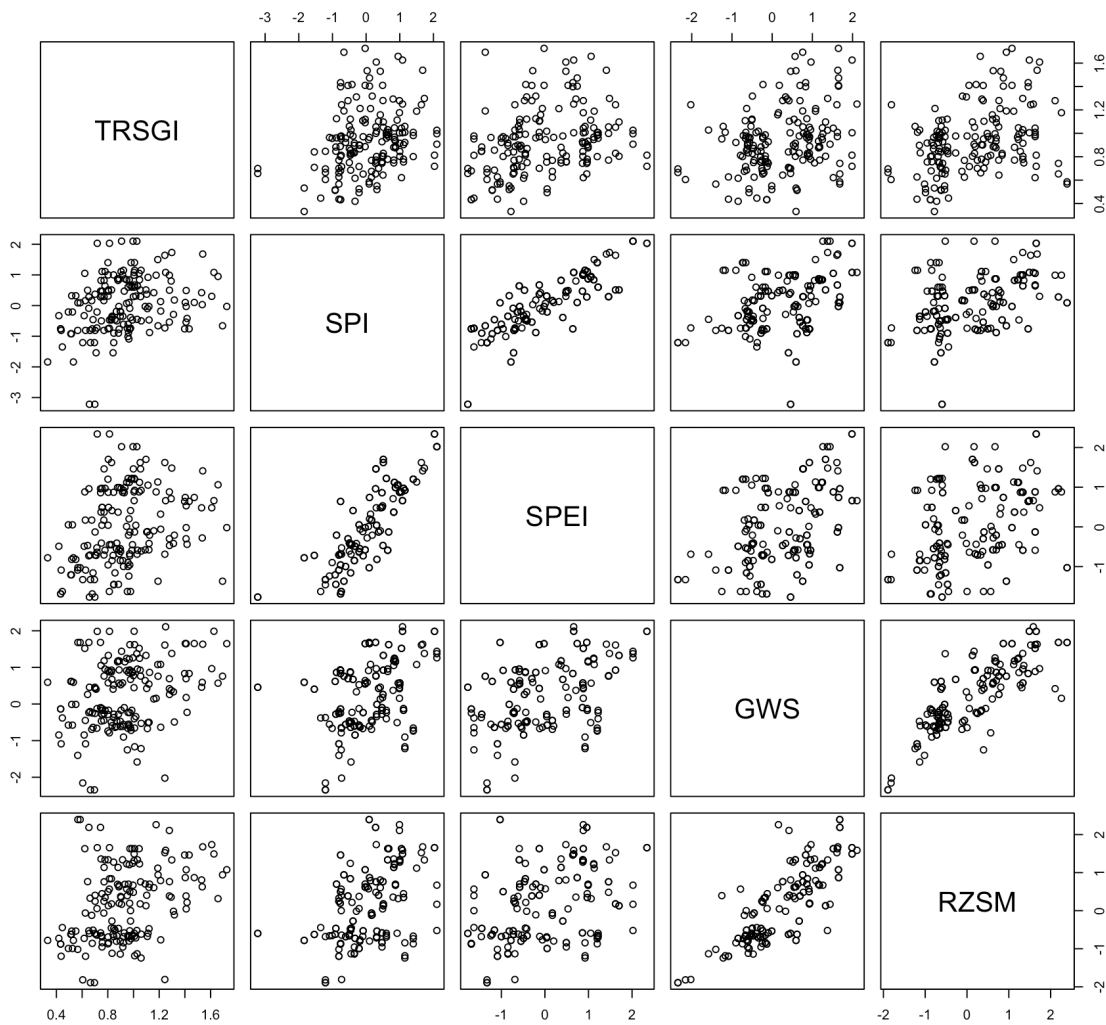


Figure 3.11: The scatterplot showing relationships between every two variables

Size	SPI	SPEI	GWS	RZSM
1				*
2		*		*
3		*	*	*
4	*	*	*	*

Table 3.6: The mean, median, minimum, and maximum of correlation coefficients between RSZM anomalies and SPEI in 3-month, 6-month, 9-month, 12-month, 18-month, 24-month accumulation periods

the tree-ring width. The result of the variable selection also indicates that RZSM anomalies might have the most significant relationship with tree-ring width in the study regions.

Size	Adjusted R^2	AIC	AICc	BIC	PRESS
1	0.07	-298.11	-297.97	-291.86	7.86
2	0.09	-298.76	-298.52	-289.39	7.82
3	0.08	-296.77	-296.41	-284.28	7.93
4	0.07	-294.78	-294.27	-279.16	8.07

Table 3.7: The mean, median, minimum, and maximum of correlation coefficients between RSZM anomalies and SPEI in 3-month, 6-month, 9-month, 12-month, 18-month, 24-month accumulation periods

3.5.2 Model Diagnostics

To test the quality of the model, this study calculates the residuals and slope coefficients for the proposed model, examining the standardized residuals plots of each predictor, the fitting plot, the square root plot, and the normal Q-Q plot (Figure 3.12). The P values of the two slope coefficients are 0.11 and 0.01. In the standardized residual plots, SPEI9 and RZSM anomalies are randomly distributed. However, the linearity assumption between fitted TRSGI and the actual TRSGI seems to be violated. The normal Q-Q plot is highly skewed at the right tail. Overall, this model is not valid for this study. Accordingly, the Box-Cox power transformation is used to reduce the non-linearity in this model. The function `boxcox`

in R is used to compute an optimal power for the dependent variable TRSGI. Based on the result (Figure 3.13), the previous model is modified to Equation (3.1).

$$TRSGI^{0.22} = \beta_0 + \beta_1 SPEI9 + \beta_2 RZSM + \epsilon \quad (3.1)$$

The same procedure is adopted to diagnose the new model. The P values of two slope coefficients are 0.05 and 0.02, which is considered as significant in this study. The diagnostic plots (Figure 3.14) illustrate significant improvements over the original model in terms of linearity, normality, and constant variance. Therefore, the new model is valid for the training dataset.

3.5.3 Model Validation

In order to validate the selected regression model, this study uses the testing dataset to calibrate the predictive capability. The min-max accuracy, mean absolute percentage error (MAPE), and mean squared prediction error (MSPR) are calculated to evaluate the predictive accuracy of the final model, which are 0.80, 0.28, and 0.09, respectively. These indicators indicate the model can provide reliable predictions of the tree-ring growth in the study regions with acceptable errors.

According to the predictor variables in the final model, it can also indicate that RZSM anomalies and SPEI have the most significant influences on the tree-ring width in California, Arizona, Oklahoma, and Mississippi. However, there are still some minor issues with the final model. For example, the non-linearity and the violation of constant variances might lead to prediction errors. In future work, increasing the sample size of the training dataset and adding more predictor variables could reduce errors.

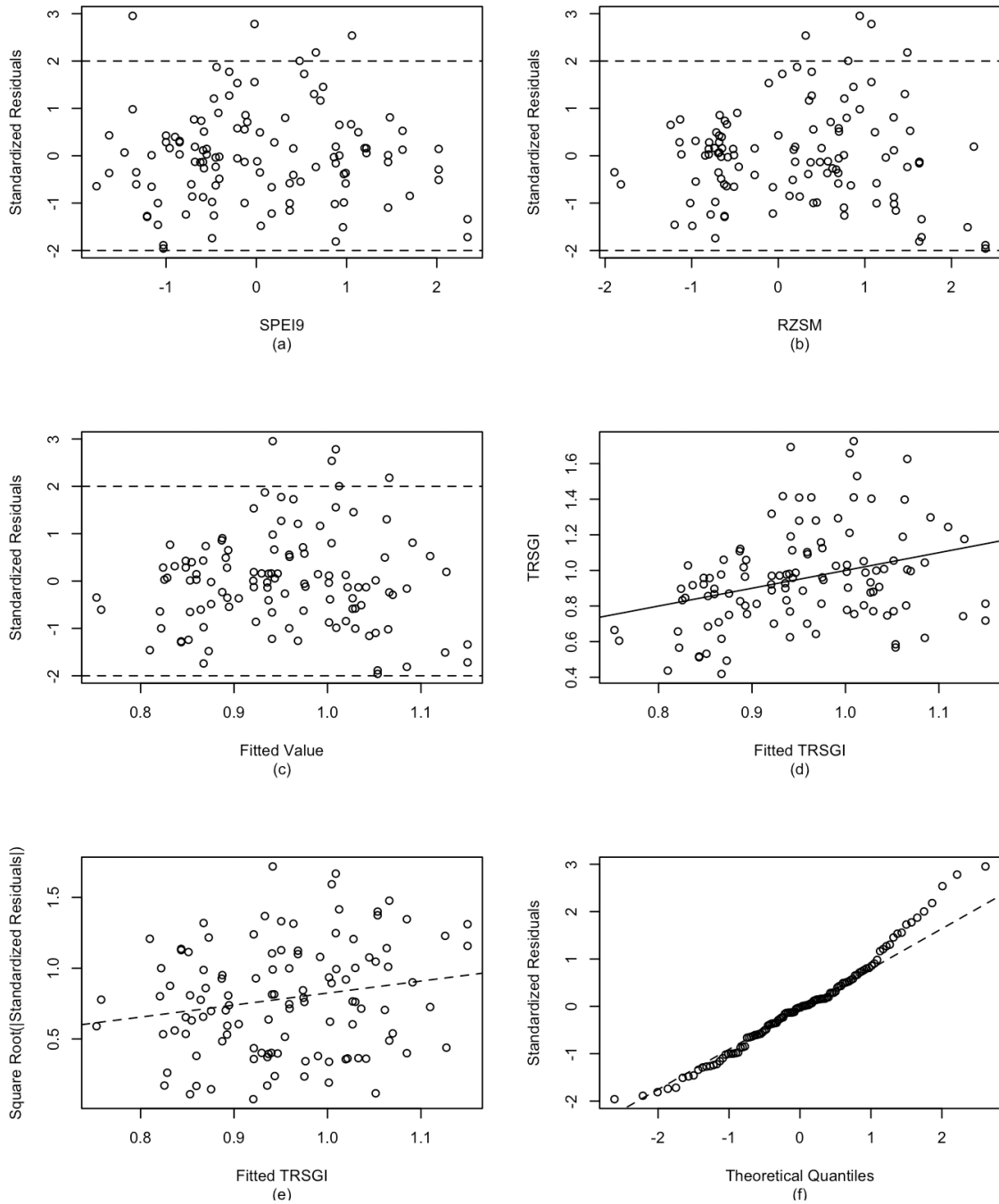


Figure 3.12: Diagnostic plots for the proposed model. (a) standardized residual plot of SPEI9 (b) standardized residual plot of RZSM anomalies (c) standardized residual plot of fitted value (fitted TRSGI) (d) Scatterplot where the x-axis is fitted TRSGI and the y-axis is actual TRSGI (e) square root plot where the x-axis is fitted TRSGI (f) normal Q-Q plot

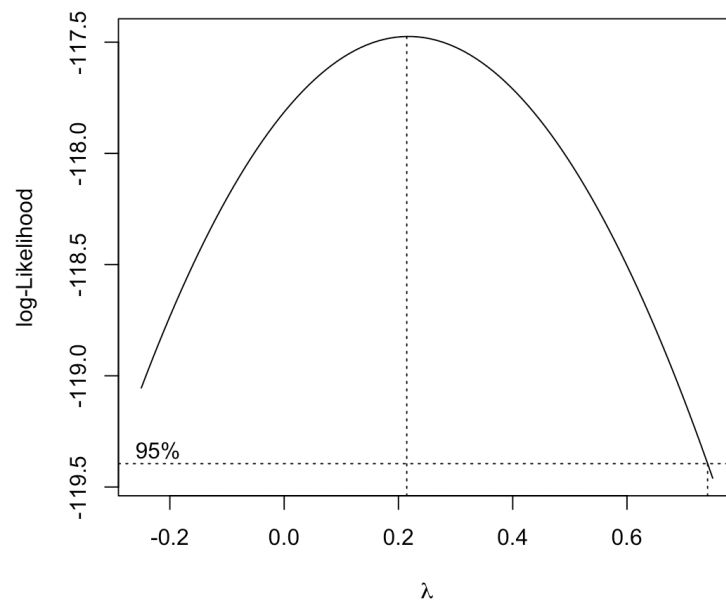


Figure 3.13: The Profile of Log-likelihood for Box-Cox Transformations

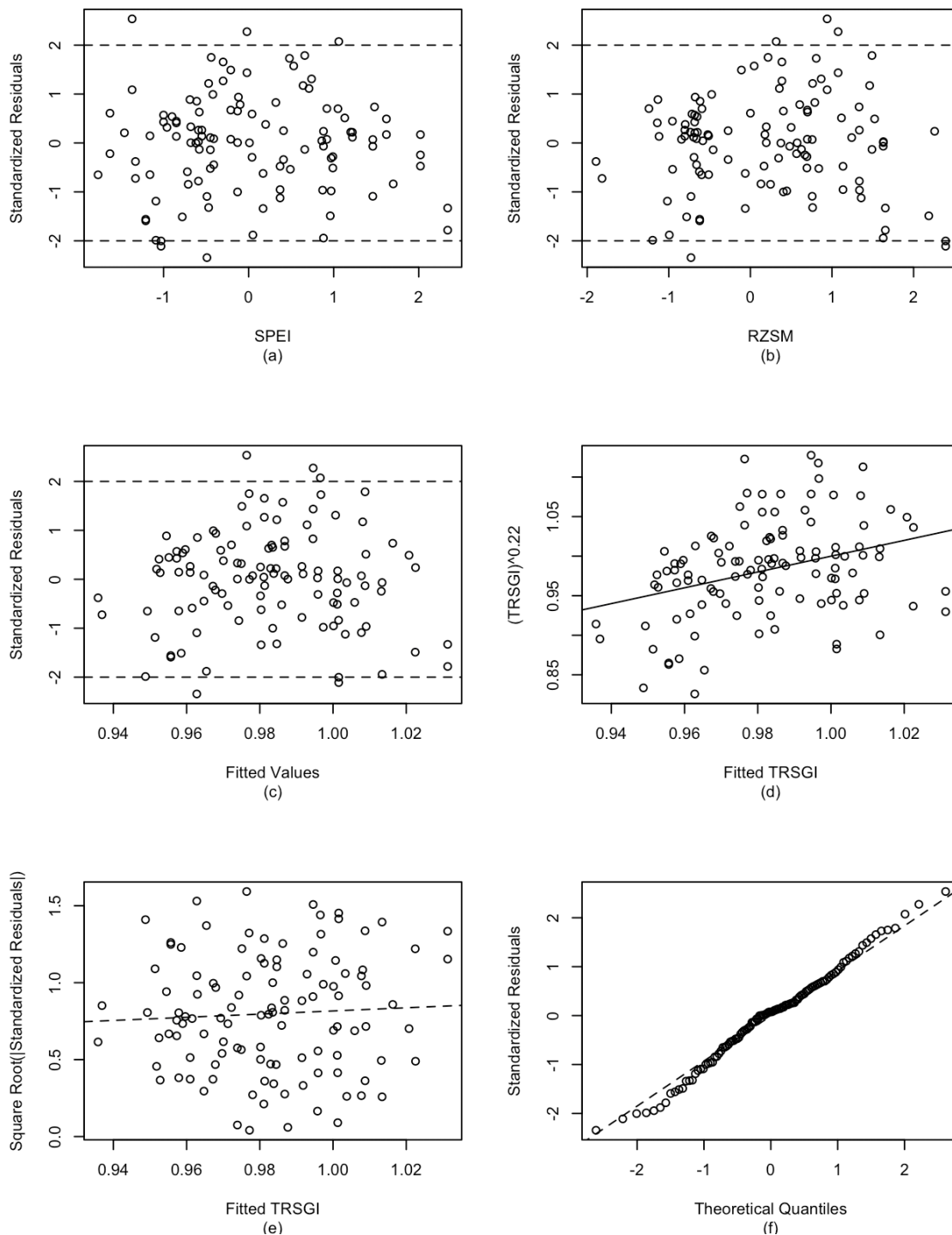


Figure 3.14: Diagnostic plots for the new model. (a) standardized residual plot of SPEI9 (b) standardized residual plot of RZSM anomalies (c) standardized residual plot of fitted value (fitted TRSGI) (d) Scatterplot where the x-axis is fitted TRSGI and the y-axis is actual TRSGI (e) square root plot where the x-axis is fitted TRSGI (f) normal Q-Q plot

Chapter 4

Conclusions

This research derives monthly GWS and RZSM anomalies from the GRACE-DA products and uses several statistical methods to calculate the correlations with commonly-used drought indicators (SPI and SPEI) and investigate the capabilities to detect the stress from drought impacts on trees at study sites. In general, this study suggests that the information from the GRACE-DA products can help to identify both short-term droughts (< 3 months) and long-term droughts (> 9 months) in most of the study regions. This research also suggests that monthly GWS and RZSM anomalies could provide timely and dependable information at a large spatial scale to predict and assess the forest drought stress.

The comparisons between monthly GWS anomalies and the multiple time-scale drought indices (3-month, 6-month, 9-month, 12-month, 18-month, and 24-month SPI and SPEI) match with the results of previous studies (Zhao et al., 2017; Mucia, 2018) that GWS anomalies have good correlations with long-term SPI and SPEI (over 9 months). The correlation coefficients between monthly GWS anomalies and SPI are over 0.4 when the accumulation period exceeds nine months. The correlations between monthly GWS anomalies and SPEI are better than the comparisons of SPI, which are over 0.5 from the 9-month accumulation to the 18-month accumulation. Monthly RZSM anomalies, on the contrary, have frequent fluctuations when the precipitation increases or decreases. They have relatively stronger relationships with 3-month SPI and SPEI. Both GWS anomalies and

RZSM anomalies have spatial homogeneities across the different accumulation periods. In addition, their performance highly depends on local environments such as topography, soil texture, climate, and vegetation. The geological formation, such as the aquifer types, also plays a vital role in the relationships between GWS anomalies and drought indices (SPI and SPEI). Therefore, this study suggests that decision-maker should consider the influences of local environments before they employ monthly GWS and RZSM anomalies into predicting drought events.

Through the results of comparisons between monthly GWS and RZSM anomalies and resampled TRSGI, this study suggests that monthly GWS and RZSM anomalies have good correlations with tree-ring widths. The previous study indicates that the characteristics of the geological formation and the depth of the water table could determine the effect of groundwater on the growth of trees (Gholami et al., 2015). The results in this research also suggest that they could weaken correlations between GWS anomalies and TRSGI in some areas such as the study sites in Oregon. Different responses of droughts among mixed tree species and isohydric/anisohydric features of trees also create additional interferences to quantify the impacts of GWS and RZSM anomalies on tree-ring widths. Although there are many variations in these comparisons, six out of ten states (Arizona, California, Idaho, Mississippi, Oklahoma, and West Virginia) have significant relationships between GWS anomalies and TRSGI with the significant level of 0.05 (Figure 3.9), and it increases to eight states (Arizona, California, Idaho, Mississippi, North Carolina, Oklahoma, Oregon, and West Virginia) between RZSM anomalies and TRSGI (Figure 3.10). The results also suggest that a majority of significant correlations between GWS and RZSM anomalies and TRSGI are in the late spring or the early summer. Due to the variations of the soil moisture content and the groundwater level, correlations have both negative and positive values. The absolute values of them are in a range from 0.51 to 0.96. Therefore, this study suggests that monthly GWS and RZSM anomalies can provide timely information about the growth

of trees before the end of the growing season. However, the percentage of tree sites with significant correlations is just 35.3% for the comparison of GWS anomalies and 58.8% for the comparison of RZSM anomalies. The small number of tree sites (34) and the short period of observations (8 years) could be two main reasons to have a relatively low percentage of significant sites and large variations of results.

This study uses multiple linear regression to quantify the impacts of monthly GWS and RZSM anomalies on tree-ring widths. The analysis also includes commonly-used drought indices (SPI, SPEI). The final model consists of SPEI9 and monthly RZSM anomalies. It indicates the predictive variable, monthly RZSM anomalies, is one of the most important parameters in the equation to predict the tree-ring widths. Thus, this study suggests that monthly RZSM anomalies could provide additional information to decision-makers about the stress from the drought on trees. Moreover, RZSM anomalies are collected remotely and contain information for large areas. This study suggests that considering monthly RZSM anomalies in forest drought stress detecting and monitoring could improve the decision-makers' efficiency.

Based on the results of this research, several improvements can be adopted in the future. First, the tree sites are distributed across the CONUS because of the limitation of the tree-ring database. To reduce the spatial variations, in future work, the study could focus on a national forest region or a state. Second, increasing the number of tree sites and the length of the observation period is necessary to improve the reliability of statistical results. Furthermore, station-based SPI and SPEI data could be interpolated to gridded datasets to reduce the effects of distance between weather stations and tree sites. Limiting the tree species could help investigate the various responses of soil moisture stress among different species. And the impacts of local environment could be assessed by comparing correlations of the same species in different locations. In the end, future studies need a validation process to assess the results of predictions from the GRACE-DA information. For example, prediction results

could be compared with the U.S. Drought Monitor datasets.

In the future, additional studies can be developed to investigate the relationships between environmental variables and the growth of trees. For example, long historical modeled datasets such as the Catchment land surface model could be used as input variables. Other geographic variables such as AWC could also be considered to provide supplementary information. Finally, non-linear methods can be adopted in the model selection if the non-linearity exists in future work.

Appendix A

Time Series Plots of monthly GWS anomalies, SPI, and SPEI at az597, az587 and or092



Figure A.1: The time series plot of monthly GWS anomalies and SPI3 at sites az597 and az598 (they are at a same location)

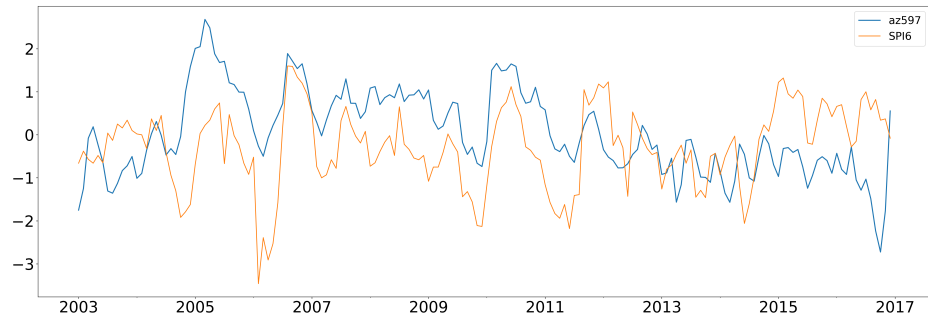


Figure A.2: The time series plot of monthly GWS anomalies and SPI6 at sites az597 and az598 (they are at a same location)



Figure A.3: The time series plot of monthly GWS anomalies and SPI9 at sites az597 and az598 (they are at a same location)

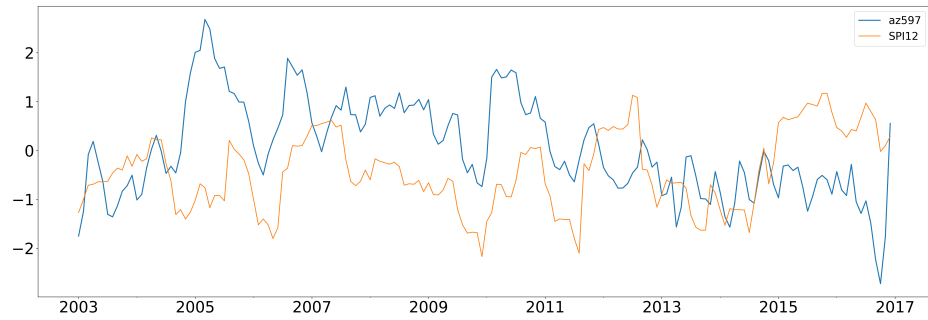


Figure A.4: The time series plot of monthly GWS anomalies and SPI12 at sites az597 and az598 (they are at a same location)

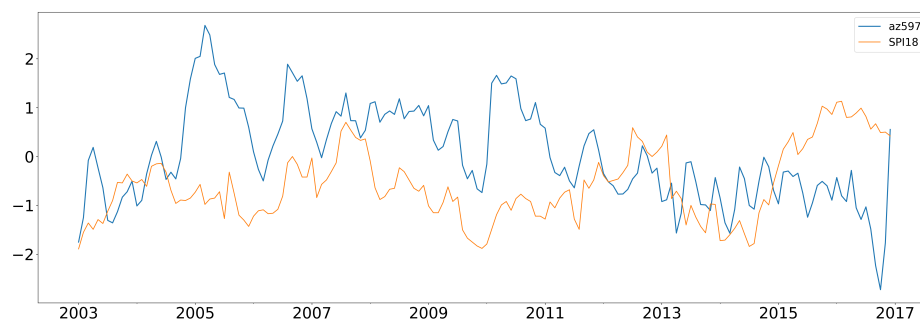


Figure A.5: The time series plot of monthly GWS anomalies and SPI18 at sites az597 and az598 (they are at a same location)



Figure A.6: The time series plot of monthly GWS anomalies and SPI24 at sites az597 and az598 (they are at a same location)

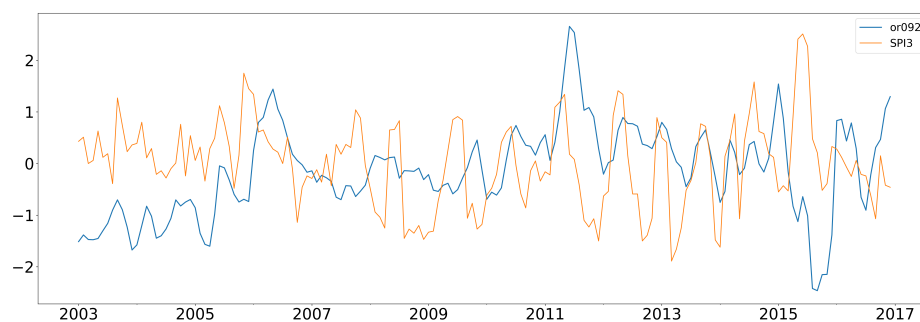


Figure A.7: The time series plot of monthly GWS anomalies and SPI3 at the site or094

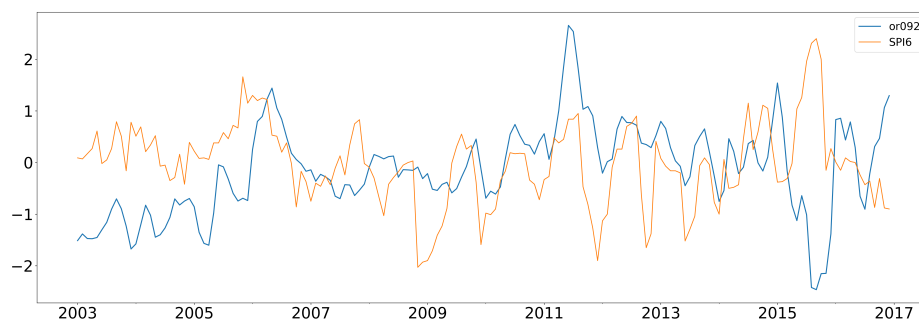


Figure A.8: The time series plot of monthly GWS anomalies and SPI6 at the site or094

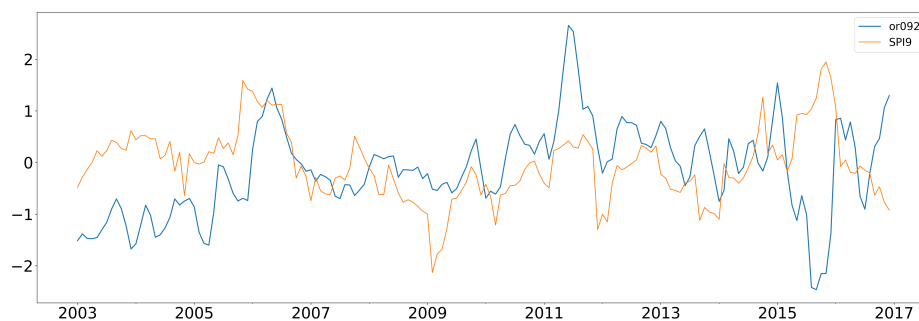


Figure A.9: The time series plot of monthly GWS anomalies and SPI9 at the site or094

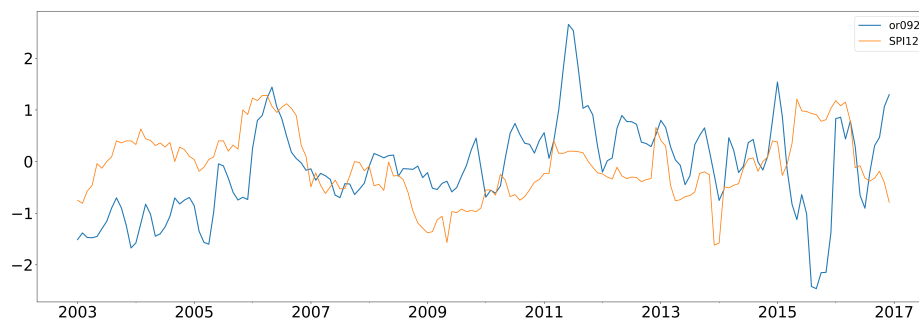


Figure A.10: The time series plot of monthly GWS anomalies and SPI12 at the site or094

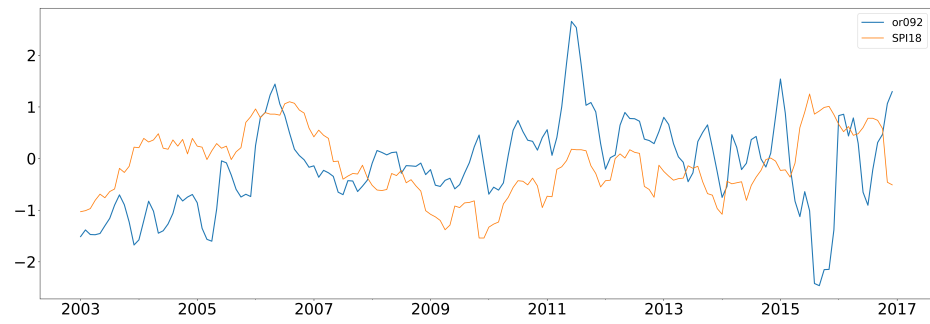


Figure A.11: The time series plot of monthly GWS anomalies and SPI18 at the site or094

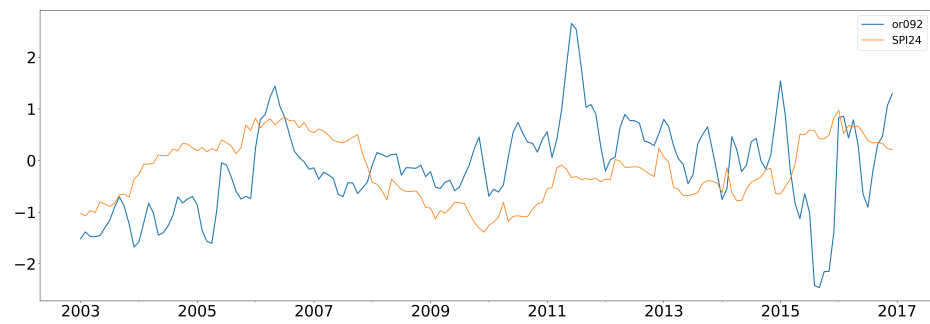


Figure A.12: The time series plot of monthly GWS anomalies and SPI24 at the site or094

Appendix B

Comparison between drought indices (SPEI and SPI) and TRSGI

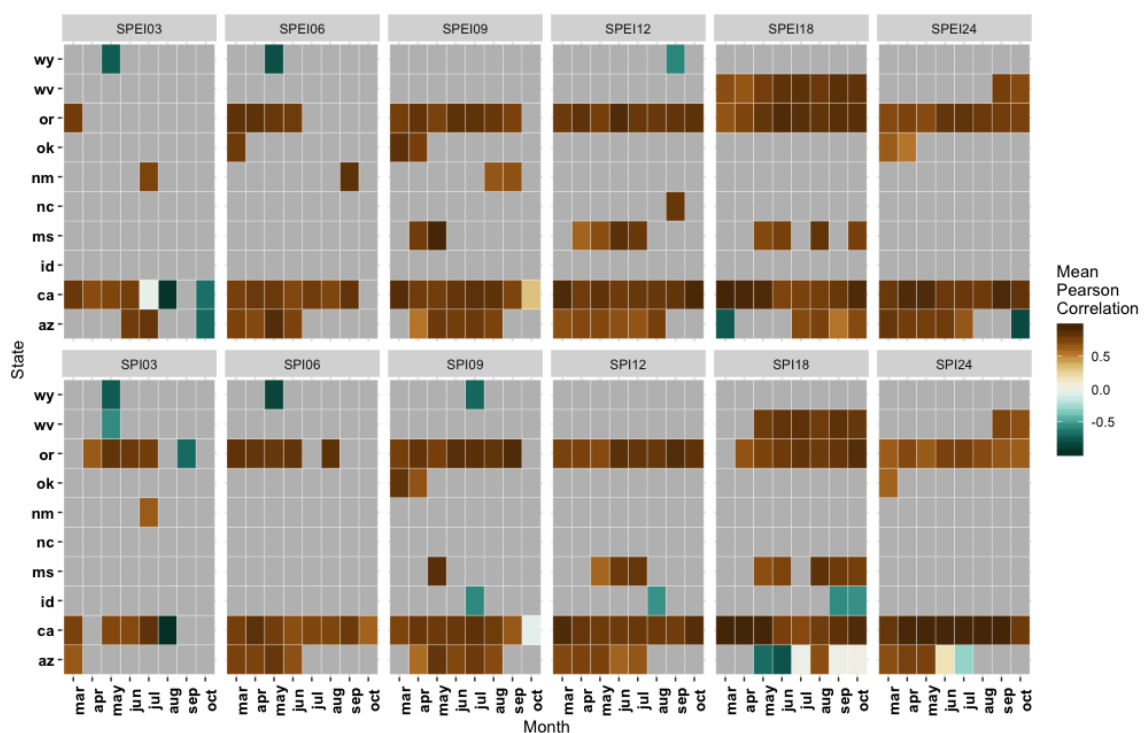


Figure B.1: The heatmap showing the correlations between drought indices (SPEI and SPI) and resampled TRSGI in ten states, where grey represents insignificant correlations, brown and black represents high positive and negative correlations respectively, and brighter color represents lower correlation

References

- Allen, C. D., Breshears, D. D., & McDowell, N. G. (2015). On underestimation of global vulnerability to tree mortality and forest die-off from hotter drought in the Anthropocene. *Ecosphere*, *6*(8), 1–55. doi: 10.1890/ES15-00203.1
- Babst, F., Poulter, B., Trouet, V., Tan, K., Neuwirth, B., Wilson, R., . . . Frank, D. (2013). Site- and species-specific responses of forest growth to climate across the European continent. *Global Ecology and Biogeography*, *22*(6), 706–717. doi: 10.1111/geb.12023
- Bayissa, Y., Tadesse, T., Demisse, G., & Shiferaw, A. (2017). Evaluation of satellite-based rainfall estimates and application to monitor meteorological drought for the Upper Blue Nile Basin, Ethiopia. *Remote Sensing*, *9*(7), 1–17. doi: 10.3390/rs9070669
- Bayissa, Y. A., Moges, S. A., Xuan, Y., Van An del, S. J., Maskey, S., Solomatine, D. P., . . . Tadesse, T. (2015). Spatio-temporal assessment of meteorological drought under the influence of varying record length: the case of Upper Blue Nile Basin, Ethiopia. *Hydrological Sciences Journal*, *60*(11), 1–16. Retrieved from <http://dx.doi.org/10.1080/02626667.2015.1032291> doi: 10.1080/02626667.2015.1032291
- Bhuyan, U., Zang, C., & Menzel, A. (2017). Different responses of multispecies tree ring growth to various drought indices across Europe. *Dendrochronologia*, *44*, 1–8. Retrieved from <http://dx.doi.org/10.1016/j.dendro.2017.02.002> doi: 10.1016/j.dendro.2017.02.002
- Chen, X., & Hu, Q. (2004, sep). Groundwater influences on soil moisture and surface evaporation. *Journal of Hydrology*, *297*(1-4), 285–300. Retrieved from <https://www.sciencedirect.com/science/article/pii/S0022169404002215> doi: 10.1016/J.JHYDROL.2004.04.019
- Dale, V. H., Joyce, L. A., McNulty, S., Neilson, R. P., Ayres, M. P., Flannigan, M. D., . . . others (2001). Climate change and forest disturbances: climate change can affect

forests by altering the frequency, intensity, duration, and timing of fire, drought, introduced species, insect and pathogen outbreaks, hurricanes, windstorms, ice storms, or landslides. *BioScience*, 51(9), 723–734.

- Dobbertin, M. (2005). Tree growth as indicator of tree vitality and of tree reaction to environmental stress: A review. *European Journal of Forest Research*, 124(4), 319–333. doi: 10.1007/s10342-005-0085-3
- Ducharne, A., Koster, R. D., Suarez, M. J., Stieglitz, M., & Kumar, P. (2000). A catchment-based approach to modeling land surface processes in a general circulation model: 2. Parameter estimation and model demonstration. *Journal of Geophysical Research: Atmospheres*, 105(D20), 24823–24838. doi: 10.1029/2000jd900328
- Eicker, A., Schumacher, M., Kusche, J., Döll, P., & Schmied, H. M. (2014). Calibration/Data Assimilation Approach for Integrating GRACE Data into the WaterGAP Global Hydrology Model (WGHM) Using an Ensemble Kalman Filter: First Results. *Surveys in Geophysics*, 35(6), 1285–1309. doi: 10.1007/s10712-014-9309-8
- Fritts, H. (2012). *Tree rings and climate*. Elsevier.
- Gao, S., Liu, R., Zhou, T., Zhao, X., Yi, C., Luo, H., . . . Lu, R. (2018). Dynamic responses of tree-ring growth to multiple dimensions of drought. *Global Change Biology*, 24(11), 5380–5390. doi: 10.1111/gcb.14367
- Gholami, V., Chau, K. W., Fadaee, F., Torkaman, J., & Ghaffari, A. (2015). Modeling of groundwater level fluctuations using dendrochronology in alluvial aquifers. *Journal of Hydrology*, 529, 1060–1069. Retrieved from <http://dx.doi.org/10.1016/j.jhydrol.2015.09.028> doi: 10.1016/j.jhydrol.2015.09.028
- Hayes, M. (2019, July 31). personal communication.
- Hochberg, U., Rockwell, F. E., Holbrook, N. M., & Cochard, H. (2018). Iso/Anisohydry: A Plant–Environment Interaction Rather Than a Simple Hydraulic Trait. *Trends in Plant Science*, 23(2), 112–120. Retrieved from <http://dx.doi.org/10.1016/>

j.tplants.2017.11.002 doi: 10.1016/j.tplants.2017.11.002

- Houborg, R., Rodell, M., Li, B., Reichle, R., & Zaitchik, B. F. (2012). Drought indicators based on model-assimilated Gravity Recovery and Climate Experiment (GRACE) terrestrial water storage observations. *Water Resources Research*, *48*(7). doi: 10.1029/2011WR011291
- Jeong, S. J., Ho, C. H., Gim, H. J., & Brown, M. E. (2011). Phenology shifts at start vs. end of growing season in temperate vegetation over the Northern Hemisphere for the period 1982-2008. *Global Change Biology*, *17*(7), 2385–2399. doi: 10.1111/j.1365-2486.2011.02397.x
- Khaki, M., Hoteit, I., Kuhn, M., Awange, J., Forootan, E., van Dijk, A. I., . . . Pattiaratchi, C. (2017). Assessing sequential data assimilation techniques for integrating GRACE data into a hydrological model. *Advances in Water Resources*, *107*, 301–316. doi: 10.1016/j.advwatres.2017.07.001
- Koster, R. D., Suarez, M. J., Ducharne, A., Stieglitz, M., & Kumar, P. (2000). A catchment-based approach to modeling land surface processes in a general circulation model: 1. Model structure. *Journal of Geophysical Research: Atmospheres*, *105*(D20), 24823–24838. doi: 10.1029/2000jd900328
- Kumar, R., Musuza, J. L., Van Loon, A. F., Teuling, A. J., Barthel, R., Ten Broek, J., . . . Attinger, S. (2016). Multiscale evaluation of the Standardized Precipitation Index as a groundwater drought indicator. *Hydrology and Earth System Sciences*, *20*(3), 1117–1131. doi: 10.5194/hess-20-1117-2016
- Landerer, F. W., & Swenson, S. (2012). Accuracy of scaled grace terrestrial water storage estimates. *Water resources research*, *48*(4).
- Li, B., & Rodell, M. (2015). Evaluation of a model-based groundwater drought indicator in the conterminous U.S. *Journal of Hydrology*, *526*, 78–88. Retrieved from <http://dx.doi.org/10.1016/j.jhydrol.2014.09.027> doi: 10.1016/j.jhydrol.2014.09

.027

- Li, B., Rodell, M., Zaitchik, B. F., Reichle, R. H., Koster, R. D., & van Dam, T. M. (2012). Assimilation of GRACE terrestrial water storage into a land surface model: Evaluation and potential value for drought monitoring in western and central Europe. *Journal of Hydrology*, *446-447*, 103–115. Retrieved from <http://dx.doi.org/10.1016/j.jhydrol.2012.04.035> doi: 10.1016/j.jhydrol.2012.04.035
- Long, D., Scanlon, B. R., Longuevergne, L., Sun, A. Y., Fernando, D. N., & Save, H. (2013). GRACE satellite monitoring of large depletion in water storage in response to the 2011 drought in Texas. *Geophysical Research Letters*, *40*(13), 3395–3401. doi: 10.1002/grl.50655
- Ma, Y., Liu, Y., Song, H., Sun, J., Lei, Y., & Wang, Y. (2015). A standardized precipitation evapotranspiration index reconstruction in the taihe mountains using tree-ring widths for the last 283 years. *PLoS ONE*, *10*(7), 1–15. doi: 10.1371/journal.pone.0133605
- Masson-Delmotte, V., Zhai, P., Pörtner, H., Roberts, D., Skea, J., Shukla, P., . . . others (2018). Ipcc, 2018: Summary for policymakers. *Global warming of, 1*.
- Mckee, T. B., Doesken, N. J., & Kleist, J. (1993, nov). THE RELATIONSHIP OF DROUGHT FREQUENCY AND DURATION TO TIME SCALES. In *Eighth conference on applied climatology*. Retrieved from <https://climate.colostate.edu/pdfs/relationshipofdroughtfrequency.pdf> doi: 10.1002/joc.846
- Mitchell, K. E., Lohmann, D., Houser, P. R., Wood, E. F., Schaake, J. C., Robock, A., . . . others (2004). The multi-institution north american land data assimilation system (nldas): Utilizing multiple gcip products and partners in a continental distributed hydrological modeling system. *Journal of Geophysical Research: Atmospheres*, *109*(D7).
- Nasa. (2003). Studying the Earth's Gravity from Space: The Gravity Recovery and Climate Experiment (GRACE). *NASA Facts*, 1–6.

- North, E. (2019, June 23). personal communication.
- Ogaya, R., Barbeta, A., BaÅşnou, C., & Peñuelas, J. (2015). Satellite data as indicators of tree biomass growth and forest dieback in a Mediterranean holm oak forest. *Annals of Forest Science*, 72(1), 135–144. doi: 10.1007/s13595-014-0408-y
- Perry, T. O. (1989). Tree roots: facts and fallacies. *Arnoldia*, 49(4), 3–29.
- readme for grace data assimilation outputs using the catchment fortuna-2.5*. (2017, June 12). Retrieved from ftp://gs617-rio.gsfc.nasa.gov/pub/DM/UT050_3M_v01
- Rowlands, D. D., Luthcke, S. B., Klosko, S. M., Lemoine, F. G., Chinn, D. S., McCarthy, J. J., . . . Anderson, O. B. (2005). Resolving mass flux at high spatial and temporal resolution using GRACE intersatellite measurements. *Geophysical Research Letters*, 32(4), 1–4. doi: 10.1029/2004GL021908
- Scanlon, B. R., Longuevergne, L., & Long, D. (2012). Ground referencing GRACE satellite estimates of groundwater storage changes in the California Central Valley, USA. *Water Resources Research*, 48(4), 1–9. doi: 10.1029/2011WR011312
- Su, H., Yang, Z. L., Dickinson, R. E., Wilson, C. R., & Niu, G. Y. (2010). Multisensor snow data assimilation at the continental scale: The value of Gravity Recovery and Climate Experiment terrestrial water storage information. *Journal of Geophysical Research Atmospheres*, 115(10), 1–14. doi: 10.1029/2009JD013035
- Sun, S., Sun, G., Caldwell, P., McNulty, S., Cohen, E., Xiao, J., & Zhang, Y. (2015). Drought impacts on ecosystem functions of the U.S. National Forests and Grasslands: Part II assessment results and management implications. *Forest Ecology and Management*, 353, 269–279. Retrieved from <http://dx.doi.org/10.1016/j.foreco.2015.04.002> doi: 10.1016/j.foreco.2015.04.002
- Tangdamrongsub, N., Han, S. C., Tian, S., Schmied, H. M., Sutanudjaja, E. H., Ran, J., & Feng, W. (2018). Evaluation of groundwater storage variations estimated from GRACE data assimilation and state-of-the-art land surface models in Australia and

- the North China Plain. *Remote Sensing*, 10(3), 1–26. doi: 10.3390/rs10030483
- Tapley, B., Watkins, M. M., Flechtner, F., Reigber, C., Bettadpur, S., Rodell, M., . . . Velicogna, I. (2019). Contributions of GRACE to understanding climate change. *Nature Climate Change*, 9(May). Retrieved from <http://dx.doi.org/10.1038/s41558-019-0456-2> doi: 10.1038/s41558-019-0456-2
- Tapley, B. D., Bettadpur, S., Ries, J., Thompson, P. F., & Watkins, M. M. (2004). Grace measurements of Mass variability in the Earth system: supporting online material. *Science*, 503-505(5683), 503–506.
- Thomas, B. F., Famiglietti, J. S., Landerer, F. W., Wiese, D. N., Molotch, N. P., & Argus, D. F. (2017). GRACE Groundwater Drought Index: Evaluation of California Central Valley groundwater drought. *Remote Sensing of Environment*, 198, 384–392. Retrieved from <http://dx.doi.org/10.1016/j.rse.2017.06.026> doi: 10.1016/j.rse.2017.06.026
- Tree ring data description*. (n.d.). Retrieved from <ftp://ftp.ncdc.noaa.gov/pub/data/paleo/treering/treeinfo.txt>
- Vicente-Serrano, S. M., Beguería, S., & López-Moreno, J. I. (2010). A multiscalar drought index sensitive to global warming: The standardized precipitation evapotranspiration index. *Journal of Climate*, 23(7), 1696–1718. doi: 10.1175/2009JCLI2909.1
- Vicente-Serrano, S. M., Camarero, J. J., & Azorin-Molina, C. (2014). Diverse responses of forest growth to drought time-scales in the Northern Hemisphere. *Global Ecology and Biogeography*, 23(9), 1019–1030. doi: 10.1111/geb.12183
- Vose, J., Clark, J. S., Luce, C., & Patel-Weynand, T. (2016). Effects of drought on forests and rangelands in the united states: a comprehensive science synthesis. *Gen. Tech. Rep. WO-93b*. Washington, DC: US Department of Agriculture, Forest Service, Washington Office, 93, 1–289.
- Wells, N., Goddard, S., & Hayes, M. J. (2004). A Self-Calibrating Palmer Drought Severity

- Index. *American Meteorological Society*, 2335.
- Wilhite, D. A. (1993). The Enigma of Drought. *Drought Assessment, Management, and Planning: Theory and Case Studies*, chap. 1, pp. 3–15. Retrieved from <http://digitalcommons.unl.edu/droughtfacpub/65> doi: DOIhttps://doi.org/10.1007/978-1-4615-3224-8_1
- Wilhite, D. A. (2000). Drought as a Natural Hazard: Concepts and Definitions. *Drought: A Global Assessment*, 147–162.
- Wilhite, D. A., Glantz, M. H., & And Glantz, M. H. (1985). Understanding the Drought Phenomenon: The Role of Definitions. *Water International*, 111–120. Retrieved from <http://digitalcommons.unl.edu/droughtfacpub><http://digitalcommons.unl.edu/droughtfacpub/20> doi: 10.1080/02508068508686328
- Wilhite, D. A., Sivakumar, M. V. K., & Pulwarty, R. (2014). Managing drought risk in a changing climate: The role of national drought policy. *Weather and Climate Extremes*, 3(March 2013), 4–13. Retrieved from <http://dx.doi.org/10.1016/j.wace.2014.01.002> doi: 10.1016/j.wace.2014.01.002
- Williams, A. P., Allen, C. D., Macalady, A. K., Griffin, D., Woodhouse, C. A., Meko, D. M., . . . Others (2012). Temperature as a potent driver of regional forest drought stress and tree mortality. *Nature Climate Change*, 3(3), 292–297. Retrieved from <http://dx.doi.org/10.1038/nclimate1693> doi: 10.1038/nclimate1693
- Yeh, P. J., Swenson, S. C., Famiglietti, J. S., & Rodell, M. (2006). Remote sensing of groundwater storage changes in Illinois using the Gravity Recovery and Climate Experiment (GRACE). *Water Resources Research*, 42(12), 1–7. doi: 10.1029/2006WR005374
- Zaitchik, B. F., Rodell, M., & Reichle, R. H. (2008). Assimilation of GRACE Terrestrial Water Storage Data into a Land Surface Model: Results for the Mississippi River Basin.

- Journal of Hydrometeorology*, 9(3), 535–548. Retrieved from <http://journals.ametsoc.org/doi/abs/10.1175/2007JHM951.1> doi: 10.1175/2007JHM951.1
- Zargar, A., Sadiq, R., Naser, B., & Khan, F. I. (2011). A review of drought indices. *Environmental Reviews*, 19(NA), 333–349. Retrieved from <http://www.nrcresearchpress.com/doi/abs/10.1139/a11-013> doi: 10.1139/a11-013
- Zhao, M., A, G., Velicogna, I., & Kimball, J. S. (2017). A Global Gridded Dataset of GRACE Drought Severity Index for 2002–2014: Comparison with PDSI and SPEI and a Case Study of the Australia Millennium Drought. *Journal of Hydrometeorology*, 18(8), 2117–2129. doi: 10.1175/jhm-d-16-0182.1